A STUDY ON MAGNETIC PROPERTIES OF NiO AND MnO BY USING DENSITY FUNCTIONAL APPROXIMATION

CHEWA THASSANA

A THESIS SUBMITTED IN PARTIAL FULFILLMENT

OF THE REQUIREMENT FOR THE DEGREE OF

PHILOSOPHY IN APPLIED PHYSICS

FACULTY OF SCIENCE

KING MONGKUT'S INSTITUTE OF TECHNOLOGY LADKRABANG

2012

KMITL-2012-SC-D-030-005

หัวข้อวิทยานิพนธ์	การศึกษาสมบัติทางแม่เหล็กของนิเกิลออกไซด์และแมกานิสออกไซด์ด้วยวิธีการประมาณฟังก์ชันความหนาแน่น
นักศึกษา	นายชีวะ ทัศนา
รหัสประจำตัว	49067051
ปริญญา	ปรัชญาดุษฎีบัณฑิต
สาขาวิชา	ฟิสิกส์ประยุกต์
พ.ศ.	2554
อาจารย์ที่ปรึกษา	รองศาสตราจารย์วิชาญ เตชิตธีระ

บทคัดย่อ

งานวิจัยนี้เป็นการศึกษาผลของการเปลี่ยนแปลงค่าของอันตรกิริยาคูลอมบ์ อันตรกิริยาแลกเปลี่ยนและการบีบอัดปริมาตรต่อสมบัติทางแม่เหล็กของนิเกิลออกไซด์และแมกานิสออกไซด์ด้วยวิธีการประมาณฟังก์ชันความหนาแน่นร่วมกับอันตรกิริยาคูลอมบ์ ซึ่งผลการคำนวณ พบว่าค่าของสปินและออร์บิทัลแมกเนติกโมเมนต์ของทั้งนิเกิลออกไซด์และแมกานิสออกไซด์จะมีแปรผันตามการเปลี่ยนแปลงของอันตรกิริยาคูลอมบ์และอันตรกิริยาแลกเปลี่ยน แต่จะแปรผกผันกับการบีบอัดทางปริมาตร และพบว่าเมื่อมีการบีบอัดทางปริมาตรเพิ่มขึ้นจนถึง 50% โดยปริมาตร ค่าสปินแมกเนติกโมเมนต์ของนิเกิลออกไซด์จะไม่ปรากฏให้เห็น และการบีบอัดที่ 70% โดยปริมาตร ค่าสปินแมกเนติกโมเมนต์ของแมกานิสออกไซด์จะไม่ปรากฏให้เห็น ยิ่งไปกว่านั้นถ้าทำการบีบอัดปริมาตรจนถึง 80% โดยปริมาตร พบว่าค่าของสปินและออร์บิทัลแมกเนติกโมเมนต์ของวัสดุทั้งสองจะหายไปอย่างสิ้นเชิง

ผลการศึกษาความสัมพันธ์ระหว่างสปินแมกเนติกโมเมนต์และออร์บิทัลแมกเนติกโมเมนต์กับอันตรกิริยาคูลอมบ์ในช่วง 0 ถึง 10 อิเล็กตรอนโวลต์ พบว่า มีความสัมพันธ์กันแบบเชิงเส้นเขียนเป็นสมการได้เป็น $m_s = 0.03U + 1.60\ \mu_B$ และ $m_o = 0.03U + 0.14\ \mu_B$ ตามลำดับ และยังพบว่าเมื่อทำการเพิ่มการบีบอัดจนถึง 150 จิกะปาสคาล ปริมาตรของยูนิตเซลล์จะลดลงถึง 30% เป็นผลให้ค่าคงที่แลตทิซลดลงจาก 0.419 นาโนเมตร เป็น 0.372 นาโนเมตร ซึ่งส่งผลให้ค่าสปินแมกเนติกโมเมนต์ของนิเกิลออกไซด์ลดลงจาก 1.78 เป็น 1.65 โบร์แมกนีตรอน และค่าออร์บิทัลแมกเนติกโมเมนต์ลดลงจาก 0.16 เป็น 0.10 โบร์แมกนีตรอน

ในขณะเดียวกันผลการศึกษาแมกานิสออกไซด์ด้วยวิธีเดียวกันกับนิเกิลออกไซด์ พบว่าค่าสปินแมกเนติกโมเมนต์ขึ้นอยู่กับค่าของอันตรกิริยาคูลอมบ์และอันตรกิริยาแลกเปลี่ยนด้วยเช่นกันกับกรณีนิเกิลออกไซด์ ทั้งนี้เมื่อค่าอันตรกิริยาคูลอมบ์เพิ่มขึ้น 10% จะส่งผลให้ค่าสปินแมกเนติกโมเมนต์เพิ่มขึ้นประมาณ 0.2 % ในขณะที่อันตรกิริยาแลกเปลี่ยนเพิ่มขึ้น 10 % จะส่งผลให้ ค่าของสปินแมกเนติกโมเมนต์เพิ่มขึ้นประมาณ 1.0% ทั้งนี้ความสัมพันธ์ระหว่างค่าของสปินแมกเนติกโมเมนต์กับค่าอันตรกิริยาคูลอมบ์และค่าอันตรกิริยาแลกเปลี่ยนสามารถเขียนเป็นสมการได้เป็น $m_s = 0.02U + 4.55\ \mu_B$. และ $m_s = 0.10J + 4.60\ \mu_B$ ตามลำดับ นอกจากนี้ค่าของสปินแมกเนติกโมเมนต์ยังเป็นฟังก์ชันของการบีบอัดทางปริมาตรด้วยเช่นกัน เมื่อการบีบอัดทางปริมาตรเพิ่มขึ้นทุกๆ 10% ค่าสปินแมกเนติกโมเมนต์จะมีค่าลดลง 1.2 % แต่ถ้ามีการบีบอัดทางปริมาตรเกิน 70% ค่าความเป็นแม่เหล็กจะหายไปอย่างสิ้นเชิงด้วยเช่นกัน

Thesis Title	A Study on Magnetic Properties of NiO and MnO by using Density Functional Approximation
Student	Chewa Thassana
Student ID	49067051
Degree	Philosophy of Doctor
Program	Applied Physics
Year	2011
Thesis Advisor	Assoc. Prof. Wicharn Techitdheera

ABSTRACT

In this work, The effect of the Coulomb interaction U, the exchange interaction J and the volume compression (VC) on both spin (m_s) and orbital (m_o) magnetic moment of NiO and MnO were studied by using the local spin density approximation plus the Coulomb interaction $(LSDA+U)$ within the full potential linear muffin-tin orbital (FP-LMTO). Our calculated results showed the both spin and orbital magnetic moment of NiO and MnO strongly correlated to U, J and VC. The relevant results exhibited the increasing magnetic moments with increasing Coulomb interaction, exchange interaction and decreasing volume compression. The interesting behavior appeared when volume compression was greater than 70% for NiO and 50% for MnO at which m_s collapsed. Moreover increasing of volume compression to be at 80% lead to the disappearance of both spin and orbital magnetic moments.

Magnetic moments of NiO were evaluated as function of Coulomb interaction U, the relation of magnetic moments and Coulomb interaction could be expressed as $m_s = 0.03U + 1.60\ \mu_B$ and $m_o = 0.03U + 0.14\ \mu_B$. Both spin and orbital magnetic moments depended strongly on the Coulomb interaction U in range of 0 to $10\,eV$. The spin and orbital magnetic moments gradually increased to $1.87\ \mu_B$ and $0.17\ \mu_B$, respectively. As the pressure raised from atmosphere pressure to 150 GPa resulted in decreasing the volume from 0 to 30% and the lattice constant from 4.19 Å to 3.72 Å. These significant decreasing could consequently effect to the decrease in spin and orbital magnetic moments from $1.78\ \mu_B$ to $1.65\ \mu_B$ and $0.16\ \mu_B$ to $0.10\ \mu_B$, respectively.

On the other hand, it was also found that the spin magnetic moment of MnO depend on Coulomb interaction U and the exchange interaction J as those of NiO, the 10% change of U could change about 0.2% in the spin magnetic moment. We could define $m_s = 0.02U + 4.55\mu_B$ ($J = 0.89eV$). In addition , the spin magnetic moment–exchange interaction ($m_s - J$) relation was $m_s = 0.10J + 4.60\mu_B$ ($U = 6.9eV$). Furthermore, the spin magnetic moments of MnO was found to decrease with increasing VC. At the compression range of 0 -50%, the m_s decreases from its original value by 1.2% as the VC increases by 10%. As the VC is larger than 70%, the spin magnetic moment of MnO rapidly decreases to zero.

ACKNOWLEDMENTS

I would like to express my deepest gratitude to my advisor Assoc. Prof Wicharn Techitdheera for his constantly moral support, guidance, invaluable suggestion and entirely positive encourangement during my study program at KMITL. During the course of my research, I have received courage from my parent and my girlfriend.

I would also like to especially thank Nakhon Ratchasima Rajabhat University (NRRU) for their financial support.

Finally, I wish to express my gratitude to my beloved parent and all the members of my family (Poo, Nat, Pla and my grandmother Ya-RAM) for their constant love and moral support, Definitely, I can't finish my program without them, accordingly this work is also dedicated to them.

CHEWA THASSANA

LIST OF PUBLICATIONS

International Journals :

1. **C. Thassana** and W. Techitdheera, **The Coulomb interaction and volume compression effect on spin and orbital magnetic moment of NiO**, J. Nanoscience and Nanotechnology, **Vol. 11, No 12,** pp 10900-10903(2011)

2. **C. Thassana** and W. Techitdheera, **Coulomb and Exchange Interaction Effect on Magnetic Properties of MnO"**, J. Applied Mechanics and Materials. **Vols. 110-116,** pp 492-496(2012)

International Proceedings :

1. **C. Thassana** and W. Techitdheera, **Coulomb and Exchange Interaction Effect on Magnetic Properties of MnO"**, International Conference on Physics Science and Technology (ICPST 2011), December 26-28,2010, pp 185-187, Hongkong, 2010

2. **C. Thassana** and W. Techitdheera , **The Effect of Coulomb Interaction and Exchange Interaction on Spin Magnetic Moment of MnO**, Proceedings of 14th International Annual Symposium on Computational Science and Engineering (ANSCSE 14)", March 23-26, 2010, pp341-344, Chiang Rai, Thailand,2010

TABLE OF CONTENTS

PAGE

TABLE OF CONTENTS (cont.)

PAGE

TABLE OF CONTENTS (cont.)

PAGE

TABLE OF CONTENTS (cont.)

PAGE

LIST OF TABLES

TABLE **PAGE**

IST OF FIGURES

FIGURE **PAGE**

LIST OF FIGURES (cont.)

FIGURE **PAGE**

CHAPTER 1

INTROCUTION

1.1 Motivation

Over decades, many researchers interested in the electronic structures and the magnetic properties of transition metal monoxides (TMO), such as MnO, FeO, CoO and NiO, have been widely investigated both experimentally and theoretically. Among these compounds, NiO and MnO are one of the most potentially applicable compound being used in variety of applications for instance high-temperature superconductors [1], and electrochromic devices [2]. It is widely accepted that NiO and MnO are a type II antiferromagnetic insulator, the magnetic moments are aligned ferromagnetically on the (111) plane and the Neel temperature (T_N) of 523K and 122K, respectively.[3,4]. The number of working experimental researchs have been recently dedicated to discriminate its relevant physical and magnetic properties including Coulomb interaction U [5], the magnetic moments [6,7,8] and lattice parameter [9]

Previous experiments gave the total magnetic moment of NiO is equal to $1.64\,\mu_B$ [6], $1.77\,\mu_B$ [7], $1.90\,\mu_B$ [8] and MnO is $4.58\,\mu_B$ [10]. Meanwhile, theoretical studies on NiO and MnO have been accordingly carried out by various calculation methods including the local spin density approximation plus Coulomb interaction U (LSDA+U) [11, 12], the local spin density approximation plus dynamical mean-fields theory (LSDA+ DMFT) [13], the self-interaction correction local spin density approximation (SIC-LDA) [14, 15], SIC+LDA+U [16, 17], Constrained LDA [18], and so on.

The purpose of this thesis is testing the LSDA+U by evaluating the ground state properties of some transition metal monoxides i.e. NiO and MnO. To this end we have used the LSDA+U with a full potential linear muffin-tin orbital (FP-LMTO) method to study the effect of the Coulomb interaction U and exchange interaction J on both spin and orbital magnetic moments of NiO and MnO. In addition, we also studied the effect of volume compression on magnetic properties of NiO and MnO.

1.2 State of the problems

Although the electronic and magnetic properties of NiO and MnO have been studied within LSDA+U method by many pioneered works, but the effect of the Coulomb interaction U, exchange interaction J and the volume compression VC on the spin and orbital magnetic moments have not yet been investigated. Thereby, in this work, we report on the pioneered study focusing on the effect of the parameter U, J and the VC on the spin and orbital magnetic moment of NiO and MnO by using the LSDA+U approximation within FP-LMTO method.

1.3 Objective

To study the effect of the Coulomb interaction U, the exchange interaction J and volume compression VC on the spin and orbital magnetic moment of antiferromagnetic type II NiO and MnO.

1.4 Scope of this study

In this work, We study the effect of the Coulomb interaction U, exchange interaction J and volume compression on the magnetic properties of NiO and MnO by using the local spin density approximation plus Coulomb interaction $(LSDA+U)$ within full potential linear muffin-tin orbital (*FP-LMTO*). The first scope is to study, the effect of the Coulomb interaction U on spin and orbital magnetic moment of NiO and MnO. The next is to study, the effect of the exchange interaction J on spin and orbital magnetic moment of NiO and MnO. Finally, to study effect of volume compression or pressure on the magnetic properties of NiO and MnO.

1.5 Dissertation outline

The outline of this dissertation is as follows; chapter 1 is an overview of the research motivation, statement of the problem, objectives and scope of this research. In chapter 2 we will mention about the background of transition metal monoxide (TMO), which it consist the introduction to transition metal monoxide (TMO), electronic structure and magnetic properties of NiO and MnO.

In Chapter 3, the LSDA+U and its implementation within full potential linear muffin-tin orbital (FP-LMTO) are introduced. We start from a brief historical overviews about this theoretical method. The we will explain the meaning of phrase as follow Coulomb interaction, the exchange interaction and the volume compression.

In chapter 4 and 5 we give an account of the calculation details, results and discussion, which is starting point for performing the preparing control files for calculation the magnetic properties of NiO and MnO, respectively. Then our calculated results were described in chapter 5, we focus on the effect of Coulomb interaction U and exchange interaction J on the magnetic properties of NiO and MnO and calculated the effect of the volume compression on their magnetic properties.

Finally, We will conclude the overall work and outlines the direction of the future work in chapter 6.

References:

[1] M. Rubinstein, R.H. Kodama, S.A. Makhlouf, J Magn Magn Mater. 2234, 289 (2001).

[2] H. Liu, W. Zheng, X. Yan, and B. Feng, J. Alloy Compd. 462, 356(2008).

[3] C.G. Shull, W.A. Strauser, and E.O. Wollan, J. Phys. Rev. 83, 333 (1951).

[4] J. Baruchel, M. Schlenker, K. Kurosawa, and S. Saito, J. Philos. Mag. B 43, 853 (1981).

[5]. J.C. Fuggle, G.A. Sawatzky, J.W. Allen, B. Brandow, Narrow Band Phenomena, (Plenum, New York, 1988).

[6]. H. A. Alperin, J. Phys. Soc. Jpn. Suppl. B. 17,12 (1962).

[7]. I. Barin, Thermochemical Data of Pure Substance, (VCH- Cambrige,1989).

[8]. B.E.F. Fender, A.J. Jacobson, F.A. Wedgewood, J. Chem. Phys. 48, 990 (1968).

[9] R. W. G. Wyckoff, Crystal Structure, Interscience, New York, 1964.

[10] A.K. Cheetham and D.A. Hope, J. Phys. Rev B, 27, pp 6964-6967, 1983.

[11] Tuo Cai, Huilei Han , You Yu , Tao GaO, Jiguang Du and Liangghuan Hao, J. Physica B 404, 89 (2009).

[12] S.K. Kwon and B.I. Min, J. Phys. Rev. B 62, 73(2000)

[13] O. Miura and T Fujiwara, J. Phys. Rev. B 77, 195124 (2008).

[14] A. Svane Du and O. Gunnarsson, J. Lett.65,vol 9, pp 1148-1151, 1990.

[15] Z. Szotek, and .W.M. Temmerman, J. Phys. Rev.B.47, vol 7, 4029-4032, 1992.

[16] V.I. Anisimov, J Zaanen and O.K Anderson, J. Phys. Rev. B, 44, vol 3, pp 943-954, 1991.

[17] D.W. Boukhvalov, A.I. Lichtenstein and V.I. Anisimov, J Phys. Rev. B.65,pp 184435-1-1184435-6, 2002.

[18] I.A. Nekrasov, M.A. Korotin and V.I. Anisimov, "cond-mat/0009107v1.

CHAPTER 2

BACKGROUND OF TRANSITION METAL OXIDE

2.1 Introduction

In this chapter, we will briefly explain the electronic structure and basic properties of transition metal (TM) and transition metal monoxide (TMO). We first explain the main reasons for strong correlations in several classes of materials. The basic principles of transition metal and its oxide compounds are the briefly reviewed. We emphasize the NiO and MnO. In particular, the spin and orbital magnetic moment of NiO and MnO have been explained.

2.1.1 Strongly correlated materials

In this section, we give a few examples of strongly correlated materials. The discussion emphasizes a few key points but is otherwise very brief. [1, 2, 3, 4, 5] The physical properties of electrons in many solids can be described by assuming an independent particle picture. This is particularly successful when one deals with broad energy bands, associated with a large value of the kinetic energy. In this cases, the valence electrons are highly itinerant, they are delocalised over the entire solid. The typical time spent near a specific atom in the crystal lattice is very short. In such a situation, valence electrons are well described using a wave-like picture, in which individual wavefunctions are calculated from an effective one-electron periodic potential.

However, for some materials, this physical picture suffers from severe limitations and may fail altogether. This happens when valence electrons spend a larger time around a given atom in the crystal lattice and, hence have a tendency towards localisation. In such cases, electrons tend to see each other and the effects of statistical correlation between the motions of individual electrons become important. An independent particle description will not be appropriate, particularly at short or intermediate time scales. A particle-like picture may in fact be more appropriate than wave-like one over those time scales, involving wavefunctions localised around specific atomic sites. Materials, which electronic correlations are significant, are general associated with moderate values of the bandwidth or narrow bands.

2.1.2. Transition metals

The *d* block elements contain the transition metals. These are elements which form some compounds in which there is an incomplete sub-level of *d* electrons. This means that strictly speaking scandium and zinc ([Ar] $3d^0$ and [Ar] $3d^{10}$). However, they are often included as their compounds, for instance NiO, MnO, FeO and CoO, resemble those of transition metals.

In 3d transition metals, the 4s orbitals have lower energy than the 3d and are therefore filed. First, The 4s orbitals extend much further from the nucleus, and thus overlap strongly. This holds the atoms sufficiently far apart so that the *d*-orbitals have a small direct overlap. Nevertheless, *d*-orbitals extend much further from the nucleus than the core electrons, As a result, throughout the 3*d* series of transition metals, *d*-electrons do have an itinerant character, giving rise to quasiparticle bands. Screening is relatively efficient in transition metals because the 3*d* band is not too far in energy from the 4s band. The latter plays the dominant role in screening the Coulomb interaction. Charge transfer process between two neighboring atoms: $3d^n4s + 3d^n4s \longrightarrow 3d^{n-1}4s^2 + 3d^{n+1}$, [6]. For all these reasons, the band not being extremely narrow and screening being efficient, electron correlations do have important physical effects for 3d transition metals. Band structure calculations based on DFT-LDA methods overestimate the width of the occupied d-band .

2.1.3 Transition metal oxides

Transition metal oxides from a fascinating class of compounds with a wide range of technological applications. They are used in catalysis, laser, and magnetic recording tapes, as well as in sensors for very high pressures and for gases, for example, applications in magnetic-field sensors, that based on the principle of giant magnetoresistance and transparent transistors, applicable as on screen electronic devices in displays or cameras, were added recently. In addition, they are responsible for the occurrence of high-temperature superconductivity.

In transition metal compounds (oxides or nitride), the direct overlap between *d*-orbitals is generally so small that *d*-electrons can only move through hybridization with the ligand atoms e.g oxygen 2*p*-bands. The 5-fold (10-fold with spin) degeneracy of the *d*-orbitals in the atom is lifted in the solid, due to the influence of the electric field created by neighbouring atoms, i.e the ligand oxygen atoms in transition metal oxides.

For a transition metal ion in an octahedral environment, this results in a three-fold group of states (t_{2g}) which is lower in energy and a doublet (e_g) higher in energy. Indeed, the d_{xy}, d_{yz}, d_{zx} orbitals forming the t_{2g} multiplet do not point towards the ligand atoms, in contrast to the states in the e_g doublet ($d_{x^2-y^2}$, $d_{3z^2-r^2}$). The latter therefore lead to a higher cost in Coulomb repulsion energy. For a crystal with perfect cubic symmetry, the t_{2g} and e_g multiplets remain exactly degenerate, while a lower symmetry of the crystal lattice lifts the degeneracy further. For a tetrahedral environment of the transition-metalion, the opposite situation is found, with t_{2g} higher in energy than e_g In transition metals, the energy scale associated with crystal-field splitting is typically much smaller than the bandwidth.

2.2 Magnetic Moment

In this section, we discuss the prime cause of the magnetic moment within an individual atom. We will look at the properties of electronics which are of central importance to magnetism and in particular the origin of the electron's magnetic moment which is a result of its angular momentum. We also look at how the magnetic properties of electrons lead to differences in the variable energy states in the presence of a magnetic field. Finally we show how the magnetic moment of the electrons are combined to give the magnetic moment of the atom.

In classical model the angular momentum of the electrons can be used to determine the magnetic moment of the electrons by invoking the concept of electrical charge in motion. There are two contributions to the electronic magnetic moment : an orbital magnetic moment due to orbital angular momentum, and a spin magnetic moment due to electron spin.

2.2.1 Orbital magnetic moment

Let us consider the nucleus to be fixed and evaluate the orbital contribution of the electron currents to the magnetic moment of an atom.

$$m_o = \frac{1}{2c}\sum_i -er_i \times v_i \tag{2.1}$$

Where m_o is orbital magnetic moment and m_e is mass of electron, we can write

$$m_o = -\frac{e}{2m_e c}\sum_i r_i \times m_e v_i \tag{2.2}$$

We know $\sum_i r_i \times m_e v_i$ is quantized and equal to $\hbar L$, where $|L| = 0,1,2,...$ and $L_z = 0, \pm 1, \pm 2, ..., \pm L$. Thus, we have

$$\begin{aligned} m_o &= -\frac{e}{2m_e c} L \\ &= -\mu_B L \end{aligned} \tag{2.3}$$

Here, $\mu_B = \frac{e\hbar}{2m_e c} = 0.927 \times 10^{20} (ergs / gauss)$ or $\mu_B = 5.8 \times 10^{-2} (meV / T)$ is called the Bohr magneton. The Bohr magneton coresponds to the magnetic moment of a 1s electron in hydrogen atom.

2.2.2 Spin magnetic moment

In addition to orbital angular momentum $\hbar L$, each electron in an atom has an intrinsic spin angular momentum $\hbar s$, giving a total spin angular moment $\hbar S$ where

$$S = \sum_i s_i \tag{2.4}$$

The z-component of spin is $s_z = \pm \frac{1}{2}$ and the spin contribution to the magnetic moment is $\pm \mu_B$ thus, for each electron, there is a contribution $-2\mu_B s$ to the magnetic moment of an atom. If we sum over all spin, the total spin contribution to the magnetic moment is

$$m_s = -2\mu_B \sum_i s_i = -2\mu_B S \tag{2.5}$$

Note that the factor of 2 appearing in this expression is not exact. It is actually given by

$$g = 2(1 + \frac{\alpha}{2\pi} - 2.973 \frac{\alpha^2}{\pi^2} + ...) \simeq 2 \times 1.0011454$$

However, in our discussion here we will take the g-factor as 2, So, the total magnetic moment is given by

$$m_t = m_0 + m_s \tag{2.6}$$

$$m_t = -\mu_B (L + 2S) \tag{2.7}$$

2.3 Electronic and Magnetic Properties of NiO and MnO

The transition-metal monoxides MnO, CoO, and NiO form ionic, antiferromagnetic crystals with the NaCl structure [7, 8] as shown in Figure 2.1. Two transition-metal electrons saturate the O-2*p* shell, leading to O^{2-} ions with the [He] $2s^2 2p^6$ configuration and TM^{2+} ions with the [Ar]$3d^n$ configuration as follow to Table 2.1.

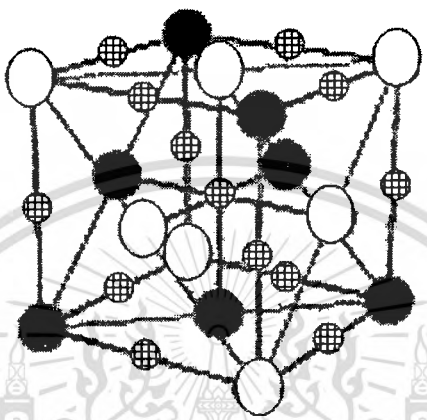

Figure 2.1 Crystal and magnetic structure of NiO and MnO ,black circles are Ni (Mn) ion spin up, white circles are Ni (Mn) spin- down and grid circles represent Oxygen ion.

Table 2.1 Electron configuration, measured insulating gap, Neel temperature, and lattice constant of MnO and NiO.

Transition metal monoxide	Electronic Configuration O^{2-}	TM^{2+}	Insulating gap (eV)	Neel Temperature (K)	Lattice Constant (nm)
MnO	[He]$2s^2 2p^6$	[Ar]$3d^5$	3.6 – 4.2	122	0.444
NiO	[He]$2s^2 2p^6$	[Ar]$3d^8$	3.1 – 4.3	523	0.419

The antiferromagnetic order of the transition-metal monoxides MnO and NiO is of that type which is often called type II antiferromagnetism in the transition-metal fcc sublattice, nearest neighbors in the [100] direction which are separated by an oxygen ion, are antiferromagnetically coupled, i.e. their spins are in opposite directions. As result, the (111) planes of the transition-metal sublattice are planes of parallel spins; adjacent (111) planes show an antiparallel alignment of the spins.

2.3.1 Electronic and magnetic properties of NiO

NiO has a rocksalt crystal structure in its paramagnetic phase. Below it's Néel temperature $T_N = 523K$, NiO is a type-II fcc antiferromagnetic compound. For this type of ordering, the magnetic moments of Ni ion align ferromagnetically on every (111) plane, and antiferromagnetically for adjacent planes, as schematically shown in Figure 2.1. Moreover, the transition from the paramagnetic state to the antiferromagnetic state is accompanied by a tiny rhombohedral distortion due to the exchange-striction effect. The lattice constant has a small increase from about 4.17 Å to 4.20 Å as the temperature increases from 7 K to 700 K.

The basic experimental facts concerning the electronic and magnetic properties of NiO are as follows: it is a good insulator with an energy gap about 4.0 eV, and this gap remains essentially unchanged above the Néel temperature (T_N) up to over 1000 K. The local magnetic moment of Ni ion is about 1.64 - 1.90 μ_B , and this value also persists unchanged above T_N.

2.3.2 Electronic structure and magnetic properties of MnO

MnO has the NaCl, rock salt structure, where cations and anions are both octahedrally coordinated. Below 118 K, MnO is antiferromagnetic.[9] MnO has the distinction of being one of the first compounds[4] to have its magnetic structure determined by neutron diffraction in 1951.[10]. This study showed that the Mn^{2+} ions form a face centered cubic magnetic sub-lattice where there are ferromagnetically coupled sheets which are anti-parallel with adjacent sheets.

The electronic structure of MnO has been investigated using high-energy (x-ray photoelectron and bremsstrahlung-isochromat) spectroscopies. An experimental gap of 3.9 eV is found. By comparing the experimental results to a configuration-interaction cluster model, values for the different parameters in a model Hamiltonian are found U = 8.5 eV. These parameter values place MnO in the intermediate region of the Zaanen-Sawatzky-Allen phase diagram. The local magnetic moment of Ni ion is about $4.58\mu_B$ [11]

References

[1] Varma, C. M., and Giamarchi, T., Model for oxide metals and superconductors, Elsevier, 1991, les Houches Summer School.

[1] Imada, M., Fujimori, A., and Tokura, Y., Rev. Mod. Phys., 70, 1039 (1998).

[3] Tsuda, N., Nasu, K., Fujimori, A., and Siratori, K., Electronic Conduction in Oxides, Springer Series in Solid-State Sciences 94, Springer, Berlin, 2000, 2nd edn., ISBN 3-540-66956-6.

[4] Mott, N. F., Metal-insulator transitions, Taylor and Francis, London, 1990.

[5]. Harrison,W. A., Electronic structure and the properties of solids, Dover Pub., New York, 1989.

[6]. Anisimov, V. I., and Gunnarsson, O., Phys. Rev. B, 43, 7570–7574 (1991).

[7]. C.G. Shull, W.A. Strauser, and E.O. Wollan, J. Phys. Rev. 83, 333 (1951).

[8]. J. Baruchel, M. Schlenker, K. Kurosawa, and S. Saito, J. Philos. Mag. B 43, 853 (1981).

[9] Greenwood, Norman N.; Earnshaw, Alan (1997). Chemistry of the Elements (2nd ed.). Oxford: Butterworth-Heinemann. ISBN 0080379419.

[10] Neutron Diffraction by Paramagnetic and Antiferromagnetic Substances C. G. Shull, W. A. Strauser, and E. O. Wollan, Phys. Rev. 83, 333 - 345 (1951)

[11] A.K. Cheetham and D.A. Hope, "Magnetic ordering and exchange effects in the antiferromagnetic solid solutions MnxNi1-xO", J. Phys. Rev B., 27, pp 6964-6967, 1983.

CHAPTER 3

DENSITY FUNCTIONAL THEORY AND LSDA+U METHOD

3.1 Introduction

Over decade, the density functional theory (DFT) developed by Kohn and Sham [1] has had a great deal of success in describing the quantum mechanical ground state of electrons in systems of interest in quantum chemistry and solid-state physics. DFT has been successfully applied to a wide range of materials in condensed matter physics, from simple elements to complex compounds, both as atoms, molecules, or three dimensional solids, as well as two dimensional interfaces and surfaces. It can in many cases accurately predict a variety of material properties. Spin-dependent exchange-correlation functionals have allowed DFT to be applied to both ferromagnetic and antiferromagnetic materials. Properties such as the equation of state (P-V curves and structural phase transitions), and the existence of magnetic phases have been succesfully and accurately computed with DFT for many materials.

In spite of DFT's successes, there exists a growing class of materials for which DFT fails to adequately describe, even qualitatively. Most of these materials contain localized d and f electrons whose contributions to exchange and correlation are not accurately computed in the commonly used local density approximation. This results in two common issues; the inaccurately calculated exchange results in a large self-interaction, and the splitting between occupied and unoccupied states ends up being too small and often zero.

A variety of approaches have been developed for overcoming the shortcomings of DFT. The most basic method is the LDA+U method, where to the DFT functional is added an orbital-dependent interaction term characterized by an energy scale U, the screened Coulomb interaction between the correlated orbitals. This method has worked well in describing several materials which fall into a class of materials termed Mott insulators. The high temperature superconducting cuprates are among the most well known successes of LDA+U. Moreover, LDA+U has also been applied to model the remarkable $Na_{1-x}CoO_2$ systems and the unusual volume and moment collapse transitions of MnO. This calculation can be done as accurately as one desires, and it is significantly cheaper in CPU time than solving a full many-body problem for all the orbitals.

3.2 Density Functional Theory (DFT)

The most important modern density functional method was developed by Kohn and Sham [1] (Kohn was awarded the Nobel prize in Chemistry in 1998.) This, along with accurate approximations of the exchange-correlation functional provide the basis for all modern calculations done with Density Functional Theory (DFT). There are many excellent references on DFT. In reference [2] provides a fairly detailed overview of DFT as well as descriptions of exchange-correlation functionals and approaches to solving numerical issues. A thorough discussion of DFT would be quite lengthy, as such we will provide an overview of DFT with references to other resources that go in depth for the interested reader.

3.2.1 Hohenberg-Kohn theorem

Hohenberg-Kohn that is a one-to-one mapping between a many-body interaction system and its ground-state density, In quantum mechanics, there is no doubt that the ground state electronic density is determined by the external potential $V(r)$. The following proof, first given by Hohenberg and Khon, is valid for systems with non-degenerate ground state and one of the most important proofs for DFT is that this relationship can be inverted [3]. That is given a ground state density the potential can be unambiguously recovered. Suppose two different external potential $V_1(r)$ and $V_2(r)$, with ground-state wavefunctions ψ_1 and ψ_2 respectively, lead to the same ground state density $n(r)$. Now it is clear that unless $V_1(r)-V_2(r)$ is constant, $\psi_1 \neq \psi_2$ since they satisfy different Schrodinger equations. Let denote the Hamiltonians and ground-state energies corresponding to ψ_1 and ψ_2 by H_1, H_2 and E_1, E_2 respectively. The two potentials lead to different Hamiltonians $H_i = K + V_i + U$, with U being an interaction term. Since ψ_2 is not the ground state of H_1. By using the minimal property of the ground-state energy. we have

$$E = \langle \psi_1 | H_1 | \psi_1 \rangle < \langle \psi_2 | H_1 | \psi_2 \rangle \tag{3.1}$$

We rewrite the last term as

$$\langle \psi_2 | H_1 | \psi_2 \rangle = \langle \psi_2 | H_2 | \psi_2 \rangle + \langle \psi_2 | H_1 - H_2 | \psi_2 \rangle \tag{3.2}$$

$$= E_2 + \langle \psi_2 | V_1 - V_2 | \psi_2 \rangle \tag{3.3}$$

$$= E_2 + \int (V_1(r) - V_2(r)) n(r) d^3r \tag{3.4}$$

giving

$$E_1 < E_2 + \int (V_1(r) - V_2(r)) n(r) d^3r \tag{3.5}$$

There]s nothing special about H_1 or H_2, so we can swap the label 1 and 2 to given

$$E_2 < E_1 + \int (V_2(r) - V_1(r)) n(r) d^3r \tag{3.6}$$

and then adding (3.5) and (3.6) gives the contradiction $E_1 + E_2 < E_1 + E_2$. Thus there cannot be two different potentials which give rise to the same ground state density; the potential must be uniquely determined by constant of $n(r)$. The Hohenberg-Kohn theorem presented here is very general. There is no assumption that the particles are fermions, bosons, identical particles, or non-interacting.

3.2.2 Kohn-Sham Approach

The key idea in modern density functional theory is to replace the interacting problem with a much simpler non-interacting problem with the density as the basic variable. The Hohenberg-Kohn theorem rigorously proves that the density can be used as the basic variable in calculating properties of the system, but does not give a framework for doing so. The Kohn-Sham approach does so by constructing an auxiliary system of non-interacting quasiparticles that have the same density as the true interacting problem. They start by assuming that there exists a system of non-interacting electrons that has the same density as the interacting system. That is, there exists some single particle potential $v_s(r)$ which when applied to non-interacting electrons, yields the same ground state density as the fully interacting problem. This assumption is justified only empirically, in fact there are a few known examples for which a Kohn-Sham system does not exist. For systems of interest in condensed matter systems, however the Kohn-Sham system always exists. The Hohenberg-Kohn theorem tells us that total energy for the interacting system can be written

$$E[n] = T[n] + U[n] + \int v_{ext}(r) n(r) d^3r \tag{3.7}$$

where $T[n]$ and $U[n]$ represent the interacting kinetic energy functional and the Coulomb potential functional for the interacting system, respectively and $v_{ext}(r)$ is the external potential.

Since we have assumed the single particle system and the interacting system have the same density, we can add and subtract $T_s[n]$ (non-interacting kinetic energy) and $E_H[n]$ (Hartree energy) to (3.7), giving

$$E[n] = T_s[n] + E_H[n] + \{T[n] - T_s[n] + U[n] - E_E[n]\} + \int v_{ext}(r)n(r)d^3r \tag{3.8}$$

$$E[n] = T_s[n] + E_H[n] + E_{xc}[n] + \int v_{ext}(r)n(r)d^3r \tag{3.9}$$

Where the exchange-correlation energy has been defined as

$$E_{xc}[n] = T[n] - T_s[n] + U[n] - E_H[n] \tag{3.10}$$

Remarkably, $E_{xc}[n]$ is a universal functional; there is no dependence on the external potential. The kinetic energy difference $T[n] - T_s[n]$ is the kinetic contribution to correlation. The difference $U[n] - E_H[n]$ is made up of Hartree-Fock exchange and the electrostatic contribution to correlation. Since the exchange correlation potential contains all the important quantum many-body effects, the true exchange correlation functional is likely to be very complex, but in many cases it can be approximated reasonably well by simple functionals.

The Hartree energy $E_H[n]$ is the classical electrostatic energy for a charge distribution $n(r)$

$$E_H[n] = \frac{1}{2}\iint \frac{n(r)n(r')}{|r - r'|} d^3r d^3r' \tag{3.11}$$

The non-interacting kinetic energy T_s is evaluated from the single particle wavwfunctions,

$$T_s[n] = \sum_i \frac{1}{2}\langle \psi[n] | p_i^2 | \psi[n] \rangle = -\sum_i \frac{1}{2}\int \psi_i^*(r)\nabla^2\psi_i(r)d^3r \tag{3.12}$$

and the density $n(r)$ and particle count N of the non-interacting system are straightfor wardly calculated as

$$n(r) = \sum_i^{occ} |\psi_i(r)|^2 \tag{3.13}$$

$$N = \int n(r)d^3r \tag{3.14}$$

We can now construct a procedure for evaluating the total energy and the single particle wavefunctions. To build in the constraint on the total number of particles, we will introduce the chemical potential (μ) as a Lagrange multiplier. To enforce orthonormality of the wavefunctions we also introduce additional Lagrange multipliers ε_{ij}. The functional to be minimized is then $E-\mu N-\sum_{ij}\varepsilon_{ij}\left(\langle\psi_i|\psi_j\rangle-\delta_{ij}\right)$ with respect to $\psi_i^*(r)$. This yields

$$\frac{\delta E-\mu N}{\delta\psi_i^*(r)}=\frac{\delta T_s[n]}{\delta\psi_i^*(r)}+v_s(r)\psi_i(r)-\mu\psi_i(r)-\sum_l\varepsilon_{ij}\psi_j(r)=0 \tag{3.15}$$

$$v_s(r)=\int\frac{n(r')}{|r-r'|}d^3r+v_{xc}(r)+v_{ext}(r) \tag{3.16}$$

In any practical application. One expands ψ_i in terms of a set of basis functions to give a matrix equation which can be diagonalized. The Kohn-Sham procedure is then as follows:

1. Guess an initial density.
2. Calculate Hamiltonian from (3.16) in the chosen basis, and diagonalize it to get the wavefunctions and band energies.
3. Fill states with N fermionic particles to determine which states are occupied.
4. Construct a new density from the wavefunctions for occupied states.
5. Mix the input and output densities for numerical stability reasons.
6. If the density hasn't converged, go to step 2.

3.2.3 Exchange Correlation Approximations,

There are a variety of approximations for the exchange-correlation functional. The most widely used ones in condensed matter physics are the local spin density approximation (LSDA). All exchange correlation functionals calculate correlation as an enhancement over exchange,

$$E_{xc}=\int n(r)v_x(r)F_{xc}(...)d^3r \tag{3.17}$$

Where F_{xc} is the enhancement and its parameters depend on whether the functional is LDA or LSDA

Local density approximation (LDA) functionals are all local functionals of density ,meaning that

$$E_{xc}^{LDA}[n] = \int f(n(r))d^3r \tag{3.18}$$

Its spin-polarized generalization, the local spin density approximation (LSDA), satisfies

$$E_{xc}^{LSDA}[n_\uparrow, n_\downarrow] = \int f(n_\downarrow(r), n_\uparrow(r))d^3r \tag{3.19}$$

The LDA approximation is designed to be exact in the limit of a uniform electron gas, so to calculate the exchange contribution, one evaluates the Fock exchange integral

$$E_x[\psi] = -\frac{1}{2}\sum_\sigma \sum_{i,j\in occ} \iint \frac{\psi_{i\sigma}^*(r)\psi_{j\sigma}^*(r')\psi_{i\sigma}(r')\psi_{j\sigma}(r)}{|r-r'|} \tag{3.20}$$

for a uniform electron gas with density n. Then one assumes that the contribution to the exchange-correlation integral (3.18) at a point r is that of a uniform gas with density $n(r)$.
This leads to the well known result

$$E_x^{LDA} = \frac{3}{4\pi}\int \left(3\pi^2 n(r)\right)^{\frac{1}{3}} n(r)d^3r \tag{3.21}$$

$$= \int \varepsilon_x(r)n(r)d^3r \tag{3.22}$$

$$\varepsilon_x(r) = \frac{3}{4}\left(\frac{3}{\pi}\right)^{\frac{1}{3}} n^{\frac{1}{3}}(r) \tag{3.23}$$

The correlation contribution is generally fit as an enhancement of exchange, in the form

$$E_{xc} = \int n(r)\varepsilon_x(r)F_{xc}(n(r))d^3r \tag{3.24}$$

taken from Monte Carlo simulations of a free electron gas. Most of the modern functionals in use are fits based off Monte Carlo data published by Ceperley and Alder [10]. Commonly used LDA correlation functionals are Vosko-Wilk-Nusair [11], M. Teter-Pade [12], and Perdew-Zunger[3]. Since these fits are all based of the Ceperley-Alder data, there is not much more than minor variation between them.

3.2.4 Local Spin Density Approximation : LSDA

A formulation of the xc functional depending only on the total electron density should allow an exact description of real materials; however the treatment of magnetic systems is much simpler if the xc energy functional is explicitly considered as dependent on the two spin populations separately. In this case the Kohn Sham equations can be written independently for the two spin polarizations:

$$\left[-\frac{\hbar^2\nabla^2}{2m}+V_{KS}^{\sigma}(r)\right]\psi_i^{\sigma}(r)=\varepsilon_i^{\sigma}\psi_i^{\sigma}(r) \tag{3.25}$$

Where we have

$$V_{KS}^{\sigma}(r)=V_{ext}(r)+e^2\int\frac{n(r')}{|r-r'|}d^3r'+v_{xc}^{\sigma}(r) \tag{3.26}$$

$$v_{xc}^{\sigma}(r)=\frac{\delta E_{xc}[n_{\uparrow},n_{\downarrow}]}{\delta n^{\sigma}(r)} \tag{3.27}$$

$$n^{\sigma}(r)=\sum_i f_i^{\sigma}\left|\psi_i^{\sigma}(r)\right|^2 \tag{3.28}$$

$$n(r)=\sum_{\sigma}n^{\sigma}(r) \tag{3.29}$$

Of course the two spin populations interact with each other through the Hartree and xc potentials and the effective field acting on one of them depends on the opposite spin charge density also. As it can be observed from the expression of the effective potential, the Coulomb part of the potential doesn't change at all with respect to LDA; the unbalance between up and down spin states, which originates the magnetization, is indeed produced by the exchange and correlation potential which accounts for the differences between like-spin and unlike-spin interactions. The exchange and correlation functionals of this generalized spin-dependent approach (whose simplest variant is the so called Local Spin Density Approximation) are usually given separate expressions. In fact, the exchange contribution is diagonal in the spin and can be obtained extending the non polarized expression:

$$E_x^{LSDA}[n] = \sum_\sigma \int F_x^{LSDA}(n_\sigma(r))d^3r = \sum_\sigma \frac{1}{2}\int F_x^{LDA}(2n_\sigma(r))d^3r \tag{3.30}$$

where F_x^{LDA} is the same functional used for the unpolarized case. The correlation functional, instead, is obtained interpolating the results for the homogeneous electron gas at different spin polarizations and can be written as dependent on both the (total) charge density $n(r)$ and the magnetization $m(r)$ which is defined as:

$$m(r) = \mu_B(n_\uparrow(r) - n_\downarrow(r)) \tag{3.31}$$

If we define the magnetic polarization,

$$\xi(r) = \frac{\frac{1}{\mu_B}|m(r)|}{n(r)} \tag{3.32}$$

So that $0 \le \xi \le 1$, this contribution to the total energy actually results:

$$E_c^{LSDA}[n,\xi] = \int\left[\varepsilon_c^U(n(r)) + f(\xi(r))\left(\varepsilon_c^P(n(r)) - \varepsilon_c^U(n(r))\right)\right]n(r)d^3r \tag{3.33}$$

where $f(\xi)$ is a smooth interpolating function with $f(0) = 0$ and $f(1) = 1$, and the ε_c^P and ε_c^U functionals represent respectively the correlation energy densities for the polarized and the unpolarized systems. The contribution to the Kohn-Sham potential coming from the exchange and correlation functionals described so far corresponds to an effective magnetic field. In fact, by calculating the first derivative of these quantities with respect to the spin polarized charge densities, we obtain a first term equal for the two spin polarizations and a second one depending on the magnetization which has the same absolute value but changes sign according to the spin it is applied on. This latter term introduces differences in the two effective fields thus producing the spin unbalances from which the magnetic properties of the system derive.

3.3 Basis sets

In practice, an application of DFT requires that the Kohn-Sham eigenstates are expanded in some finite basis set. The discussion up to this point in this chapter on DFT has been general; there have been no boundary conditions assumed. In this section we will discuss basis sets which are useful mainly for solids, so periodic boundary conditions will be assumed. There are a large variety of basis sets; a partial list of the most widely used ones would include planewaves (PW), and linear muffin-tin orbitals (LMTO). In this section, we will discuss the two basis sets that have been used most extensively in this research, which are PW and LMTO.

3.3.1 Planewaves (PW)

A basis set composed entirely of planewaves has the convenient property that with appropriate selection of planewaves, the basis automatically fulfills the periodicity condition of a crystalline solid. The Kohn-Sham eigenstate ψ_{nk} is expanded in planewaves as

$$\langle r \mid \psi_{nk} \rangle = \sum_{G} c_{n,k+G} e^{i(k+G)\cdot r} = e^{ik\cdot r} u_k(r) \tag{3.34}$$

where r is a real-space vector, and $G = \sum_i n_i b_i$ where n_i are integers and the b_i are the reciprocal lattice vectors. The satisfaction of the Bloch condition is explicit; the function $u_k(r)$ has the periodicity of the unit cell as it is composed of planewaves with wavevectors that are integer multiples of the reciprocal lattice vectors.

For a practical implementation, the basis set needs to be cut off somewhere to contain a finite number of planewaves. This is generally done with a single parameter E_{cut} which is taken as the maximum kinetic energy of any planewave used in the expansion. This results in the condition that planewaves are kept in the basis set expansion if they satisfy the condition

$$\frac{1}{2}(k+G)^2 \le E_{cut} \tag{3.35}$$

This condition represents a sphere in reciprocal space inside which points representing planewave vectors which satisfy the Bloch condition are kept in the basis expansion, and planewaves with very high kinetic energy that fall outside the sphere are discarded. In practice, a planewave

expansion is not practical to use for the basic solid problem where the atomic cores have potential $-Z/r$ and all electrons are treated on the same footing. The difficulty with the planewave basis is caused by two factors. The first complication is the treatment of highly localized core electrons. The wavefunctions for these electrons is very rapidly varying in the region near the atomic cores, and rapidly goes to zero away from the nucleus. Expanding this type of wavefunction would require a extremely large set of planewaves with extremely large kinetic energy to accurately represent these core electrons. Such a large basis set would end up being completely unwieldy computationally, and rather unnecessary as the core electrons do not play a role in many of properties of interest in solids.

The second complication for planewaves can come in expanding the core region of the valence wavefunctions, for electrons with a high principle quantum number. This is because states with different quantum numbers must be orthogonal. For electrons with the same angular momentum quantum numbers l and m_l values but principle quantum numbers n, the orthogonality cannot be taken care of by the angular part, so the radial functions must have a different number of nodes to be orthogonal. As a general rule, for hydrogenic wave functions the number of nodes in the radial wavefunction is $n-l-1$, so electrons with higher n will have extra nodes. These nodes always occur near the atomic cores in solids. Correctly capturing these nodes in a planewave basis would require a very large basis set.

The solution that is always used in planewave basis sets is to replace the atomic potential with a pseudopotential. There are a large variety of methods for generating pseudopotentials, but all of the results presented in this dissertation using planewaves were done with norm-conserving Troullier-Martins pseudopotentials [4]. These pseudopotentials are non-local [5], and can optionally include a nonlinear core correction [6]. A non-local pseudopotential contains different potentials for different orbital angular momentum values, and can be written

$$V = \sum_{lm} |lm\rangle V_l \langle lm| \tag{3.36}$$

The basic approach to generating a Troullier-Martins pseudopotential is this. One chooses which valence states should be used to generate the nonlocal potentials, and a core-radius for each is chosen. Outside this radius, the pseudopotential is exactly the atomic potential $-Z/r$, with Z equal to the number of valence electrons. Inside this radius the pseudopotential becomes a smooth function which is not divergent at $r = 0$.

3.3.2 The Linear Muffin-Tin Orbitals Method (LMTO)

The linear muffin-tin orbital (LMTO) method is one particular technique for solving the one-electron problem in crystalline solids. Among the many methods of solving band-structure problems, the LMTO method is often more favorable because it is relatively easy to implement and computationally cheap, and it has the accuracy required in most cases. In this section we first briefly review the energy band methods in general, and then discuss the LMTO method specifically. A detailed description of the LMTO method was given by Skriver (1984), which we are following here. To arrive at a final definition of LMTO, several steps are needed to take. First, instead of treating a full MT potential, we only consider a single MT well embedded in a constant potential environment. Namely we are dealing with a single-electron problem with the following potential,

$$v(r)=\begin{cases}V(r) & , \ r \le S_{MT} \\ V_{MTZ} & , \ r > S_{MT}\end{cases} \tag{3.37}$$

where $V(r)$ is the spherically symmetric potential inside the MT sphere, and V_{MTZ} is constant potential outside the sphere, with S_{MT} the radius of the MT sphere. For convenience we define

$$V_{MT}(r)=v(r)-V_{MTX}=\begin{cases}V(r)-V_{MTZ} & , \ r \le S_{MT} \\ 0 & , \ r > S_{MT}\end{cases} \tag{3.38}$$

and

$$\kappa^2 = E - V_{MTZ} \tag{3.39}$$

Therefore the Schrödinger equation of a single electron moving in the potential $v(r)$ with behaving like (3.37) reads

$$\left[-\frac{\hbar^2}{2m}+V_{MT}(r)-\kappa^2\right]\psi_L(E,r)=0 \tag{3.40}$$

Due to the spherical symmetry of the total potential $v(r)$ under consideration, the eigenfunction $\psi_L(E,r)$ can be classified by the combined angular and magnetic quantum number $L=lm$ is , and can be written as a product of a radial part and an angular part, i.e.,

$$\psi_L(E,r)=i^l Y_l^m(\hat{r})\psi_l(E,r) \tag{3.41}$$

The radial part of the Schrödinger equation satisfied by $\psi_l(E,r)$ inside the MT sphere and in the constant potential region respectively look like,

$$\left[\frac{\hbar^2}{2m}\frac{d^2}{dr^2}+\frac{l(l+1)}{r^2}+V_{MT}(r)-\kappa^2\right]r\psi_l(E,r)=0, \quad \text{for } r\le S_{MT} \tag{3.42}$$

$$\left[\frac{\hbar^2}{2m}\frac{d^2}{dr^2}+\frac{l(l+1)}{r^2}-\kappa^2\right]r\psi_l(E,r)=0, \quad \text{for } r> S_{MT} \tag{3.43}$$

Leaving Eq. (3.42) aside for a while, let us concentrate on the Helmholtz equation (3.43) which has two linearly independent solutions. For a positive κ^2, these are the spherical Bessel function $j_l(\kappa r)$ and Neumann function $n_l(\kappa r)$, and for $\kappa^2<0$, i.e., the kinetic energy is negative in the constant potential region, the Neumann function $n_l(\kappa r)$ should be replaced by the first kind Hankel function $-ih_l^{(1)}=n_l-ij_l$ Here we only present the formulations of the positive κ^2 case, and those for $\kappa^2<0$ can be obtained by a simple replacement.

Summarizing the above analysis, we can have the partial waves solving the Schrödinger equation of (3.40),

$$\psi_L(E,\kappa,r)=i^l Y_l^m(\hat{r})\begin{cases}\psi_l(\mathrm{E,r}) & r\le S_{MT}\\ \kappa\left[n_l(\kappa r)-c_l(E,\kappa)j_l(kr)\right] & r>S_{MT}\end{cases} \tag{3.44}$$

Here the coefficient $c_l(E,\kappa)$, usually expressed as $\cot(n_l(E,\kappa))$, is determined so that $\psi_L(E,\kappa,r)$ is continuous and differentiable across the boundary of the MT sphere. This requires

$$c_l(E,\kappa)=\cot(\eta_l(E,\kappa))=\frac{n_l(\kappa S_{MT})}{j_l(\kappa S_{MT})}\frac{D_l(E)-D\{n_l\}}{D_l(E)-D\{j_l\}} \tag{3.45}$$

Where

$$\begin{aligned}D\{E\}&=\frac{S_{MT}}{\psi_l(E,S_{MT})}\left.\frac{d\psi_l(E,r)}{dr}\right|_{r=S_{MT}}\\ D\{n_l\}&=\frac{S_{MT}}{n_l(\kappa S_{MT})}\left.\frac{dn(\kappa r)}{dr}\right|_{r=S_{MT}}\\ D\{j_l\}&=\frac{S_{MT}}{j_l(\kappa S_{MT})}\left.\frac{dj(\kappa r)}{dr}\right|_{r=S_{MT}}\end{aligned} \tag{3.46}$$

are the logarithmic derivative of $\psi_l(E,r)$, $n(\kappa r)$ and $j(\kappa r)$ at the sphere boundary respectively. The $\eta_l(\kappa,E)$ defined in (3.45) can be view as the phase shift of the free spherical wave for $r \to \infty$ due to the scattering of the MT potential.

The partial waves (3.44) are not suitable for serving basis functions. This is particularly because the presence of the term $-\kappa c_l(E,\kappa) j_l(\kappa r)$ in the constant potential region make them not normalizable for negative κ^2. The trick that can be employed here to cure this problem is to subtract this term from $\psi_l(E,r)$ in both regions (inside and outside the MT sphere) while maintaining the continuity and differentiability, ending up with

$$\chi_L(E,\kappa,r) = i^l Y_l^m(\hat{r}) \begin{cases} \psi_l(E,r) + \kappa c_l(E,\kappa) j_l(kr) & r \le S_{MT} \\ \kappa n_l(\kappa r) & r > S_{MT} \end{cases} \tag{3.47}$$

These orbitals $\chi_L(E,\kappa,r)$ are actually the energy dependent MTOs. Although they are not the solutions of the problem (3.40), the Bloch sum of $\chi_L(E,\kappa,r)$ and $\psi_L(E,\kappa,r)$ give the identical results except for the k points satisfying $|k+G|^2 = \kappa^2$ with G being the reciprocal lattice vector. In addition, they are reasonably localized, and regular over the whole space.

In (3.44) and (3.47), the parameter E and κ are related through Eq. (3.39). However, the continuity and differentiability of $\chi_L(E,\kappa,r)$ and $\psi_L(E,\kappa,r)$ are guaranteed by the chosen value (3.45) of $c_l(E,\kappa)$ irrespective of their possible relation between E and κ. In this connection we can disregard (3.39) and treat κ as an independent parameter. By doing so the tails of $\chi_L(E,\kappa,r)$ and $\psi_L(E,\kappa,r)$ are no longer the exact solution of the Schrödinger equation $\left[-\frac{\hbar}{2m} + V_{MT}(r) - \kappa^2\right]\psi_L(E,r) = 0$ in the region of the constant potential any more, but they have the advantage of being energy independent. Moreover, the head of $\chi_L(E,\kappa,r)$ (i.e., the part inside the MT sphere) can also be made energy independent around a fixed energy E_ν up to the first order by replacing (augmenting) $j_l(\kappa r)$ and $n_l(\kappa r)$ inside the MT sphere by more appropriate functions which are attached to the original functions at the sphere boundary in a continuous and differentiable fashion. For this purpose, we define the augmented Bessel function $j_l(\kappa r)$ as

$$J_L(\kappa r) = \begin{cases} -\dot{\psi}_l(E_\nu,r) / \kappa \dot{c}_l(E_\nu,\kappa) & r \le S_{MT} \\ j_l(\kappa r) & r > S_{MT} \end{cases} \tag{3.48}$$

where $\dot{\psi}_l$ and $\dot{c}_l$ are the energy derivative of ψ_l and c_l respectively. It is easy to verify that $J_l(\kappa r)$ defined in (3.48) is everywhere continuous and differentiable. A proper definition of the augmented Neumann function $N_l(\kappa r)$ is more delicate. Before giving an explicit form of $N_l(\kappa r)$, it is illustrating to present the following expansion theorem of $n_L(\kappa,r) = n_l(\kappa r)i^l Y_l^m(\hat{r})$ and $j_L(\kappa,r) = j_l(\kappa r)i^l Y_l^m(\hat{r})$, namely,

$$n_L(\kappa,r) = 4\pi \sum_{L'} \sum_{L''} C_{LL'L''} j_{L'}(\kappa, r-R) n^*_{L''}(\kappa,-R) \tag{3.49}$$

which is valid inside the sphere $|r| < R$. Here the Gaunt coefficients $C_{LL'L''}$ are defined as

$$C_{LL'L''} = \int Y_l^m(\hat{r}) Y_{l'}^{m'}(\hat{r}) Y_{l''}^{m''}(\hat{r}) d\hat{r} \tag{3.50}$$

The augmented spherical Neumann and Bessel functions are also required to satisfy the above expansion theorem, and this lead to the following definition of $N(\kappa r)$, including the angular part,

$$N_L(\kappa,r) = \begin{cases} 4\pi \sum_{L'} \sum_{L''} C_{LL'L''} j_L(\kappa, r-R) n^*_{L''}(\kappa,-R) \\ n_L(\kappa,r) \end{cases} \quad \begin{matrix} \\ \text{otherwise} \end{matrix} \tag{3.51}$$

To have a clear understanding of (3.51), one may think of the full MT potential composed of nonoverlapping array of MT wells: inside every MT sphere except the one where the present Neumann function is centered, $N_L(\kappa,r)$ is defined as the linear expansion of the augmented Bessel functions centered at that particular MT sphere. In other regions, both the MT sphere at the origin and the interstitial region, the augmented Neumann function is simply defined as the normal one. With $J_L(\kappa,r)$ and $N_L(\kappa,r)$ defined, we finally end up with the following definition of the augmented MTO

$$\chi_L(E,\kappa,r) = i^l Y_l^m(\hat{r}) \begin{cases} \psi_l(E,r) + \kappa c_l(E,\kappa) J_l(\kappa r) & r \le S_{MT} \\ \kappa N_l(\kappa r) & r > S_{MT} \end{cases} \tag{3.52}$$

The augmented MTO defined in (3.52) is energy independent up to the first order in $E-E_\nu$. It is everywhere continuous and differentiable, and it is orthogonal to the core states. By neglecting the high-order energy dependence of $J_L(\kappa,r)$, i.e., fixing $E=E_\nu$, we are led to the linear (energy independent) MTOs (LMTOs) $\chi_L(\kappa,r)$.

One disadvantage of the MTOs defined above is their infinite range which makes the practical calculations cumbersome. It has nevertheless been shown (Andersen and Jepsen, 1984; Andersen et al., 1986) that these conventional MTOs can be exactly transformed into a set tight-binding (TB) orbitals. These TB-MTOs, basically formed by a linear combination of the conventional ones, are rather localized and particularly suitable for first-principles electronic structure calculations.

Now we can consider solving the band structure problem with single-electron crystal potential modelled by MT approximation, within which the potential is formed by a array of MT wells centered at sites R of a three-dimensional periodic lattice. In the spirit of the LCAO method, the Bloch function can be represented as

$$\psi^k(E,r)=\sum_L \alpha_L^k(E)\chi_L^k(\kappa,r) \tag{3.53}$$

where the coefficients $\alpha_L^k(E)$ are to be determined and $\chi_L^k(\kappa,r)$ is the Bloch sum of the energy independent MTOs

$$\begin{aligned}\chi_L^k(\kappa,r)&=\frac{1}{\sqrt{\varnothing}}\sum_R e^{ik\cdot R}\chi_L(\kappa,r-R)\\&=\frac{1}{\sqrt{\varnothing}}\left(\chi_L(\kappa,r)+\sum_{R\neq 0}e^{ik\cdot R}\chi_L(\kappa,r-R)\right)\end{aligned} \tag{3.54}$$

Here $\varnothing$ is the number of the lattice sites or unitary cells. The last term in (3.54) consists of the contributions from all the MT spheres except the one at the origin. In the region that is inside the sphere centered at the origin and passing through the nearest-neighbor sites but outside the neighboring MT spheres, this term can be written as a one-center expansion,

$$\sum_{R\neq 0}e^{ik\cdot R}\chi_L(\kappa,r-R)=\sum_{R\neq 0}e^{ik\cdot R}\kappa N_L(\kappa,r-R) \tag{3.55}$$

$$=\sum_{L'}J_{L'}(\kappa,r)\beta_{L'L}^k(\kappa) \tag{3.56}$$

Where the KKR structure constants $\beta^k_{L'L}(\kappa)$, according to the expansion theorem (3.49), should be defined as

$$\beta^k_{L'L}(\kappa) = 4\pi \sum_{L''} C_{LL''L''} \sum_{R \neq 0} e^{ik\cdot R} \kappa n^*_{L''}(\kappa, R) \tag{3.57}$$

The above stated region of convergence is the intersection of the two regions where (3.55) and (3.56) are valid respectively. Therefore, inside this region, the Bloch sum of MTOs can be expressed in terms of a one-center expansion,

$$\chi^k_L(\kappa,r) = \frac{1}{\sqrt{\varnothing}} \left(\chi_L(\kappa,r) + \sum_{L'} J_{L'}(\kappa,r) \beta^k_{L'L}(\kappa) \right) \tag{3.58}$$

With the set of Bloch summed MTOs $\chi^k_L(\kappa,r)$ by applying standard variational techniques, the band structure problem is reduced to a set of linear equations at each k point

$$\sum_{L'} \left\langle \chi^k_L \mid H - E \mid \chi^k_{L'} \right\rangle \alpha^k_{L'}(E) = 0 \tag{3.59}$$

Which has solutions in case that

$$\det \left\{ \left\langle \chi^k_L \mid H - E \mid \chi^k_{L'} \right\rangle \right\} = 0 \tag{3.60}$$

Thus we need to evaluate the secular matrix element $\left\langle \chi^k_L(\kappa,r) \mid H - E \mid \chi^k_{L'}(\kappa,r) \right\rangle = 0$. Due to he translational properties of $\chi^k_L(\kappa,r)$ and H one can verify that

$$\left\langle \chi^k_L \mid H - E \mid \chi^k_{L'} \right\rangle = N \left\langle \chi^k_L \mid H - E \mid \chi^k_{L'} \right\rangle_0 \tag{3.61}$$

where $\langle\ \rangle_0$ means the integral over the atomic polyhedron at the origin. Within the atomic polyhedron, $\chi^k_L(\kappa,r)$ can be expanded as (3.58), and therefore

$$\begin{aligned} N \left\langle \chi^k_L \mid H - E \mid \chi^k_{L'} \right\rangle_0 = & \left\langle \chi_L \mid H - E \mid \chi_{L'} \right\rangle_0 \\ & + \sum_{L''} \left[\left\langle \chi_L \mid H - E \mid J_{L''} \right\rangle_0 \beta^k_{LL''} \left\langle J_{L''} \mid H - E \mid \chi_{L'} \right\rangle_0 \right] \\ & + \sum_{L''} \sum_{L'''} \beta^k_{LL''} \left\langle J_{L''} \mid H - E \mid J_{L''} \right\rangle_0 \beta^k_{L'''L'} \end{aligned} \tag{3.62}$$

For the spherically symmetric potential, the angular part of the wave functions can be first integrated out, and we are finally left with

$$\begin{aligned}\left\langle \chi_L^k \mid H-E \mid \chi_{L'}^k \right\rangle = & \left\langle \chi_l \mid H-E \mid \chi_l \right\rangle_0 \delta_{LL'} \\ & + \left[\left\langle \chi_l \mid H-E \mid J_l \right\rangle_0 + \left\langle \chi_{l'} \mid H-E \mid J_{l'} \right\rangle_0 \right] \beta_{LL'}^k \\ & + \sum_{L''} \beta_{LL''}^k \left\langle J_{l''} \mid H-E \mid J_{l''} \right\rangle_0 \beta_{L''L'}^k \end{aligned} \tag{3.63}$$

The simplification from (3.62) to (3.63) arises from the fact the secular matrix element between two $\chi_L(\kappa,r)$ or $J_L(\kappa,r)$ with two different L indices vanishes. The matrix elements appearing on the righthand side of (3.63), is defined as integrals over radial variable r, e.g.,

$$\left\langle \chi_l \mid H-E \mid \chi_l \right\rangle_0 \equiv \int_0 d^3r \; r\chi_l(\kappa,r) \left[-\frac{d^2}{dr^2} + \frac{l(l+1)}{r^2} - \kappa^2 \right] r\chi_l(\kappa,r) \tag{3.64}$$

Within the LMTO method, the integral terms on the righthand side of $\chi_L(\kappa,r)$ can be parameterized and evaluated at different orders of approximations. The detailed way of representing these integrals by a set of parameters can be found in the book of Skriver (1984). Concerning the approximations made to accomplish this, a simple and popularly used one is the so-called atomic sphere approximation (ASA), in which the κ^2 is set to 0 and the atomic polyhedra are replaced by the atomic spheres.

The procedure of constructing LMTOs described above is for the simple case when there is only one atom in a unit cell, but it could be easily extended to the multiatomic case. In that case, the LMTOs should carry one more index r distinguishing the different atoms in the unit cell, namely,

$$\chi_L^k \rightarrow \chi_{rL}^k = \chi_{rlm}^k \tag{3.65}$$

Thus in general, the LMTOs have three indices r,l,m to label the atom, the angular and magnetic quantum number.

3.4 LSDA+U Approximation

Density functional theory (DFT) and its associated local spin density approximation (LSDA) is used widely to describe the properties of a wide variety of materials, often with great success. However there exists a class of materials which are poorly described, sometimes qualitatively, by LDA. These so-called strongly correlated materials typically contain atoms with open d or f shells, in which the corresponding orbitals are in some sense localized. The LSDA+U approach was introduced by Anisimov, Zaanen, and Andersen [7] to treat correlated materials as a modification of LDA that adds an intraatomic Hubbard U repulsion term in the energy functional. Treated in a self-consistent mean field ('Hartree-Fock') manner, in quite a large number of cases the LDA+U result provides a greatly improved description of strongly correlated materials.

At the most basic level, the LSDA+U correction tends to drive the correlated orbital m occupation numbers $n_{m\sigma}$ (σ denotes spin projection) to integer values 0 or 1. This in turn produces, under appropriate conditions, insulating states out of conducting LSDA states, and the Mott insulating state of several systems is regarded as being well described by LSDA+U at the band theory level. Dudarev et al.[8] and Petukhov et al.[9] provided some description of the effect of the spin dependence of two different double counting terms within an isotropic approximation. Beyond this important but simple effect, there is freedom in which of the spin-orbitals (m_σ) will be occupied, which can affect the result considerably and therefore makes it important to understand the effects of anisotropy and spin polarization in LSDA+U. After the successes of providing realistic pictures of the Mott insulating state in La_2CuO_4 and the transition metal monoxides,[7] the anisotropy contained in the LSDA+U method produced the correct orbitally ordered magnetic arrangement for $KCuF_3$ that provided an understanding of its magnetic behavior.[10]

The anisotropy of the interaction, and its connection to the level of spin polarization, is a topic that is gaining interest and importance. One example is in the LSDA+U description of the zero temperature Mott transition under pressure in the classic Mott insulator MnO. The first transition under pressure is predicted to be [11] an insulator-insulator (not insulator-metal) transition, with a $S=\frac{5}{2}\rightarrow S=\frac{1}{2}$ moment collapse and a volume collapse. The insulator-to-insulator aspect is surprising, but more surprising is the form of moment collapse: each orbital remains singly occupied beyond the transition, but the spins of electrons in two of the orbitals

have flipped direction. This type of moment collapse is totally unanticipated, but it is robust against crystal structure occurring in both rocksalt and NiAs structures and against reasonable variation of the interaction strength. Detailed analysis indicates it is a product of the anisotropy of the LSDA+U interaction and the symmetry lowering due to antiferromagnetic order.

Another unanticipated result was obtained [12] in LaNiO2, which is a metal experimentally. This compound is also a metal in LSDA+U over a very large range of interaction strength U, rather than reverting to a Mott insulating Ni^{1+} system which would be isovalent with $CaCuO_2$. For values of U in the range expected to be appropriate for the Ni ion in this oxide, the magnetic system consists of an atomic singlet consisting of antialigned $d_{x^2-y^2}$ and d_{z^2} spins on each Ni ion. Again the anisotropy of the interaction evidently plays a crucial role in the result, with its effect being coupled thoroughly with band mixing effects.

The addition of a Hubbard U interaction also introduces the need for "double counting" correction terms in the energy functional, to account for the fact that the Coulomb energy is already included albeit more approximately in the LSDA functional. All double counting schemes subtract an averaged energy for the occupation of a selected reference state depending only on $\{N_\sigma\}$ which largely cancels the isotropic interaction of the E_I term Eq. (3.66). Several forms for these double-counting terms have been proposed,[7, 13, 14] but primarily two are commonly used. The common approach has been to use LSDA for correlated materials and include a double-counting correction. There are techniques being developed which do not build on a correction to DFT-LDA, but it remains to be seen whether these approaches will be successfully applied to a broad range of solid-state materials.

The LDA+U functional is usually coded in a form in which the choice of coordinate system is irrelevant, often referred to as the rotationally-invariant form.[10] This form involves Coulomb matrix elements that have four orbital indices, and the orbital occupation numbers are matrices in orbital space (viz. nmm'). One can always (after the fact) rotate into the orbital Hilbert space in which the occupations are diagonal, in which case the interactions have only two indices. In our discussion we will work in the diagonal representation.

The LDA+U functionals considered here can all be written in the form

$$\Delta E = E_I - E_{dc} \tag{3.66}$$

Where the direct interaction is

$$E_I = \frac{1}{2} \sum_{m\sigma \neq m'\sigma'} W_{mm'}^{\sigma\sigma'} n_{m\sigma} n_{m'\sigma'} \tag{3.67}$$

and E_{dc} is the double-counting correction. The Coulomb matrix elements are given in terms of the direct and spin-dependent exchange contributions as

$$W_{mm'}^{\sigma\sigma'} = U_{mm'} - J_{mm'}\delta_{\sigma\sigma'} \tag{3.68}$$

By the convention chosen here, E_I and E_{dc} are both positive quantities as long as the constants U and J which define the matrix elements $U_{mm'}$ and $J_{mm'}$ but are not the same as chosen conventionally, with U much larger than J.

Note that the orbital+spin diagonal term has been omitted in Eq. (3.67) there is no self-interaction in E_I. However, it is formally allowed to include the diagonal 'self-interaction' term, because the matrix element vanishes identically (self-interaction equals self-exchange: $U_{mm} = J_{mm}$), and it can simplify expressions. The double counting correction depends only on the orbital sum N_σ, which appears up to quadratic order. A consequence is that it will contain terms in $n_{m\sigma} n_{m\sigma}$, which are self-interactions. Thus while the LSDA+U method was not intended as a self-interaction correction method, it is not totally self-interaction free. In fact, the underlying LSDA method also contains self-interaction, and the double-counting term may serve to compensate somewhat this unwanted effect

The LSDA+U method is actually a class of functionals. Each functional has the same form of interaction E_I, with differences specified by

(1) choice of the form of double counting term.

(2) choice of constants U and J. For a given functional, these are 'universal' constants

(3) choice of projection method to determine the occupation matrices from the Kohn-Sham orbitals. Given identical choices for (1) and (2) above, there will be some (typically small) differences in results from different codes due to the projection method.

The occupation numbers (or, more generally, matrices) are functionals of the density, $mm\sigma[n]$, through their dependence on the Kohn-Sham orbitals. Then, whereas in LSDA one uses the functional derivative

$$LSDA: \frac{\partial E_{LSDA}[\{n_s\}]}{\partial n_\sigma(r)} \tag{3.69}$$

in minimizing the functional, in LSDA+U the expression generalizes to

$$LSDA+U \quad : \quad \frac{\partial\left(E_{LSDA}\left[\{n_s\}\right]+\Delta E\left[\{n_{ms}\left[n_s\right]\}\right]\right)}{\partial n_\sigma(r)} \tag{3.70}$$

Since the resulting spin densities n_s are changed by including the ΔE correction, the change in energy involves not only ΔE but also the change in E_{LSDA}. In practice, there is no reason to compare E_{LSDA+U} with E_{LSDA} as they are such different functionals. However, in the following we will be assessing the importance of the choice of the double counting term in the LSDA+U functional, and it is of interest to compare, for fixed U and J, the energy differences between LSDA+U functionals differing only in their double counting terms in order to understand the differing results. Even if the set of occupation numbers turn out to be the same the densities n_σ will be different and the differences in E_{LSDA} may become important.

As with the non-kinetic energy terms in E_{LSDA}, the functional derivatives of ΔE lead to potentials in the Kohn-Sham equation. These are non-local potentials, which (via the same projection used to define the occupation numbers) give rise to orbital-dependent (nonlocal) potentials

$$v_{m\sigma} \equiv \frac{\partial \Delta E}{\partial n_{m\sigma}} = v^{I}_{m\sigma} - v^{dc}_{m\sigma}$$

where

$$v^{I}_{m\sigma} = \sum_{m'\sigma' \neq m\sigma} W^{\sigma\sigma'}_{mm'} n_{m'\sigma'} \tag{3.71}$$

The corresponding contribution to the eigenvalue sum E_{sum} is

$$\Delta E_{sum} = \sum_{m\sigma} v_{m\sigma} n_{m\sigma} \tag{3.72}$$

which is subtracted from the eigenvalue sum to obtain the Kohn-Sham kinetic energy. However, there are indirect effects of the orbital potentials that affect all of the kinetic and (LSDA) potential energies; these will be different for different ΔE functionals because the orbital potentials, which depend on the derivative of ΔE and not simply on the values of $n_{m\sigma}$, differ for each functional. This makes it necessary, for understanding the effects of the ΔE correction and the change in energy, to analyze the orbital potentials.

3.5 Coulomb Interaction *U*

It is helpful to clarily briefly several points that are essential to a proper definition of energies in extended systems with long-range Coulomb interaction. The key points are : Any extended system must be neutral if the energy is to be finite. Terms in the energy must be organized in neutral groups for actual evaluation.

The most convenient approach is to identify and group together terms responding the classical Coulomb energies,

$$E^{CI} = E_{Hartree} + \int d^3 r V_{ext}(r) n(r) + E_{II} \tag{3.73}$$

Where $E_{Hartree}$ is the self-interaction energy of the density $n(r)$ treated as a classical charge density.

$$E_{Hartree} = \frac{1}{2} \int d^3 r d^3 r' \frac{n(r) n(r')}{|r - r'|} \tag{3.74}$$

Since E_{II} is the interaction among the positive nuclei and $\int d^3 r V_{ext}(r) n(r)$ is the interaction of the electron with the nuclei (3.73) is a neutral grouping of the terms so long as the system is neutral. Evaluation of classical Coulomb energies is an intrinsic part of the quantitative electronic structure calculations.

It then follows that the total energy expression, $E = \left\langle \hat{T} \right\rangle + \left\langle \hat{V}_{\text{int}} \right\rangle + \int d^3 r V_{ext}(r) n(r) + E_{II}$ can be written as

$$E = \left\langle \hat{T} \right\rangle + \left(\left\langle \hat{V}_{\text{int}} \right\rangle - E_{Hartree} \right) + E^{CI} \tag{3.75}$$

Where each of the three terms is well defined. The middle term in brackets, $\left\langle \hat{V}_{\text{int}} \right\rangle - E_{Hartree}$ is the difference between the Coulomb energies of interacting, correlated electrons with density $n(r)$ and that of a continuous classical charge distribution having the same density, which is defined to be the potential part of the exchange-correlation energy E_{XC} in density functional theory.

3.6 Exchange Interaction *J*

A quantum-mechanical phenomenon that gives the energy of two elementary particles. Exchange effects arise for all kinds of elementary particles, but these effects were first introduced into physics in consideration of atomic structure and the energy of the electrons in an atom. In this context, they arise as a consequence of two facts: electrons are indistinguishable, and they obey the Pauli exclusion principle.

When the spins of the two electrons are parallel the spatial part of the wave function is antisymmetric under exchange, and when they are opposed it is symmetric. The distribution in space of the two electrons is different in these two states, and so their mutual electrostatic energy is different. This difference in the electrostatic energy, called the exchange energy, appears as an interaction between the two electrons which depends on their relative orientation although this dependence is incidental. Exchange is the mechanism by which the electron spins in many magnetic materials are lined up parallel or opposed

Now we will discuss the exchange interactions in ferromagnetic bodies. This interaction should be analyzed by means of quantum theory, since it strongly concerns with spin-spin interactions. More specifically, on a scale in the order of the atomic scale, the exchange interaction tends to align neighbor spins. In view of a continuum average analysis in terms of magnetization vector field, we expect that the exchange interactions tends to produce small uniformly magnetized regions, indeed observed experimentally and called magnetic domains.

Magnetism can be divided into two groups, group A and group B. In group A there is no interaction between the individual moments and each moment acts independently of the others. Diamagnets and paramagnets belong to this group. Group B consists of the magnetic materials most people are familiar with, like iron or nickel. Magnetism occurs in these materials because the magnetic moments couple to one another and form magnetically ordered states. The coupling, which is quantum mechanical in nature, is known as the exchange interaction and is rooted in the overlap of electrons in conjunction with Pauli's exclusion principle. Whether it is a ferromagnet, antiferromagnet of ferrimagnet the exchange interaction between the neighboring magnetic ions will force the individual moments into parallel (ferromagnetic) or antiparallel (antiferromagnetic) alignment with their neighbours. The three types of exchange which are currently believed to exist are a direct exchange, an indirect exchange, a double exchange and a superexchange.

3.6.1. Direct exchange

Direct exchange operates between moments, which are close enough to have sufficient overlap of their wavefunctions. It gives a strong but short range coupling which decreases rapidly as the ions are separated. An initial simple way of understanding direct exchange is to look at two atoms with one electron each. When the atoms are very close together the Coulomb interaction is minimal when the electrons spend most of their time in between the nuclei. Since the electrons are then required to be at the same place in space at the same time, Pauli's exclusion principle requires that they possess opposite spins. According to Bethe and Slater the electrons spend most of their time in between neighboring atoms when the interatomic distance is small. This gives rise to antiparallel alignment and therefore negative exchange. (antiferromagnetic)

Figure 3.1. Antiparallel alignment for small interatomic distances.

If the atoms are far apart the electrons spend their time away from each other in order to minimize the electron-electron repulsion. This gives rise to parallel alignment or positive exchange (ferromagnetism), Figure 3.2.

Figure 3.2. Parallel alignment for large interatomic distances.

For direct inter-atomic exchange j can be positive or negative depending on the balance between the Coulomb and kinetic energies. The Bethe-Slater curve represents the magnitude of direct exchange as a function of interatomic distance. Cobalt is situated near the peak of this curve, while chromium and manganese are on the side of negative exchange. Iron, with its sign depending on the n crystal structures probably around the zero-crossing point of the curve.

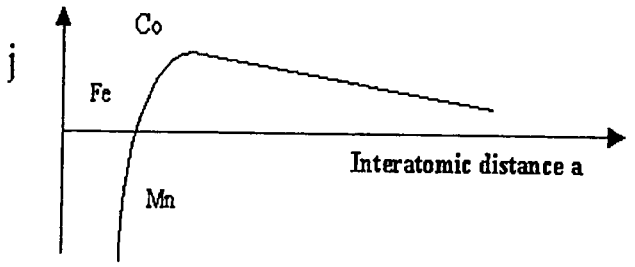

Figure 3.3 The Bethe-Slater curve.

3.6.2 Indirect exchange

Indirect exchange couples moments over relatively large distances. It is the dominant exchange interaction in metals, where there is little or no direct overlap between neighboring electrons. It therefore acts through an intermediary, which in metals are the conduction electrons (itinerant electrons). This type of exchange is better known as the RKKY interaction named after Ruderman, Kittel, Kasuya and Yoshida. The RKKY exchange coefficient j oscillates from positive to negative as the separation of the ion changes and has the damped oscillatory nature shown in Figure 3.4. Therefore depending on the separation between a pair of ions their magnetic coupling can be ferromagnetic or antiferromagnetic. A magnetic ion induces a spin polarization in the conduction electrons in its neighborhood. This spin polarization in the itinerant electrons is felt by the moments of other magnetic ions within the range leading to an indirect coupling. In rare-earth metals, whose magnetic electrons in the 4f shell are shielded by the 5s and 5p electrons, direct exchange is rather and indirect exchange via the conduction electrons gives rise to magnetic order in these materials.

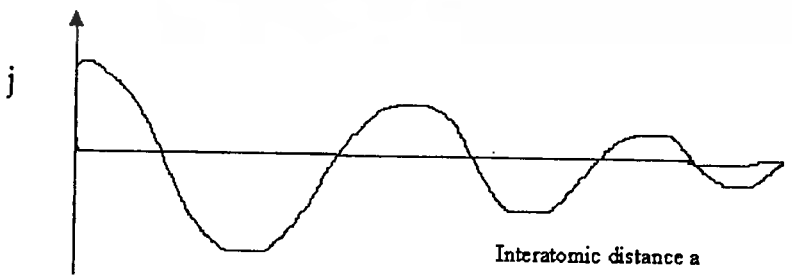

Figure 3.4. The coefficient of indirect (RKKY) exchange versus the interatomic spacing a.

3.6.3 Double-exchange

The double-exchange mechanism, first proposed by Clarence Zener, is a theory that predicts the relative ease with which an electron may be exchanged between two species, and has important implications for whether materials are ferromagnetic, antiferromagnetic, or neither. For example, consider the 180 degree interaction of Mn-O-Mn in which the Mn "e_g" orbitals are directly interacting with the O "2p" orbitals.

Hence, double-exchange predicts that electron movement from one species to another will be facilitated more easily if the electrons do not have to change spin direction in order to conform with Hund's rules when on the accepting species. The ability to hop (to delocalize) reduces the kinetic energy. Hence the overall energy saving can lead to ferromagnetic alignment of neighboring ions.

Figure 3.5 Double exchange interaction of Mn.

This model is superficially similar to superexchange. However, in superexchange, a ferromagnetic or antiferromagnetic alignment occurs between two atoms with the same valence (number of electrons); while in double-exchange, the interaction occurs only when one atom has an extra electron compared to the other.

3.6.4 Superexchange

Superexchange describes the interaction between moments on ions too far apart to be connected by direct exchange, but coupled over a relatively long distance through a non-magnetic material. We take as an example the coupling between the moments on a pair of metal cations separated by a diatomic anion as illustrated in Figure 3.6. The ferric ion has a half filled

3d shell and so has a spherically symmetric charge distribution (S state ion). The triply rare-earth ion is not symmetric and has a strong spin-orbit coupling; its charge distribution is coupled to its moment. The ion's moments are coupled via superexchange, so turning the Fe moment alters the overlap of the R cation in the molecule. This changes the magnitude of both the Coulomb and exchange interactions between the cations, leading to a coupling, which depends on the moment's orientation.

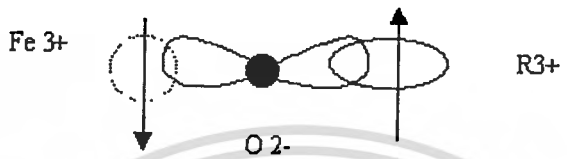

Figure 3.6. Superexchange in ferric-rare earth interaction in a garnet.

3.7 Pressure or Volume Compression and Bulk modulus.

The equation of state as a function of pressure and temperature is perhaps the most fundamental property of condensed matter. The stable structure at a given P and T determines all the other properties of the material. The total energy E at T = 0 as a function of volume Ω is the most convenient quantity for theoretical analysis because it is more straightforward to carry out electronic structure calculations at fixed volume. In essence, volume is a convenient "knob" that can be tuned to control the system theoretically. Comparison of theory and experiment is one of the touchstones of "ab initio" electronic structure research. Because direct comparison can be made with experiment, this is one of the most important tests of the state of theory, in particular, the approximations made to treat electron-electron interactions.

The fundamental quantities are energy E, pressure P, Bulk modulus B,

$$E = E(\Omega) \equiv E_{total}(\Omega) \tag{3.76}$$

$$P = -\frac{dE}{d\Omega} \tag{3.77}$$

$$B = -\Omega\frac{dP}{d\Omega} = \Omega\frac{d^2E}{d\Omega^2} \tag{3.78}$$

And higher derivatives of energy. All quantities are for a fixed number of particles, e.g. in a crystal, E is the energy per cell of volume $\Omega = \Omega_{cell}$.

The first test is to determine the theoretical prediction for the equilibrium volume Ω^0, where E is minimum or P = 0, and bulk modulus B for the known zero pressure crystal structure. Since Ω^0 and B can be measured with great accuracy (and extrapolated to T=0), this is a rigorous test for the theory. One procedure is to calculate the energy E for several values of the volume Ω, and fit to an analytic form, e.g. The Murnaghan equation of state . The minimum gives the predicted volume Ω^0 and total energy, and the second derivative is the bulk modulus B. Alternatively, P can be calculated directly from the virial theorem or its generalization and B from response functions.

References :

[1] W. Kohn and L. J. Sham. Self-consistent equations including exchange and correlation effects. Phys. Rev., 140:A1133, 1965.

[2] Richard M. Martin. Electronic Structure. The Press Syndicate of the University of Cambridge, 2004.

[3] P. Hohenberg andW. Kohn. Inhomogeneous electron gas. Phys. Rev., 136(3B):B864-B871, Nov 1964.

[4] N. Troullier and J. L. Martins. Efficient pseudopotentials for plane-wave calculations. Phys. Rev. B, 43(3):1993, 1991.

[5] Alex Zunger and Marvin L. Cohen. First-principles nonlocal-pseudopotential approach in the density-functional formalism: Development and application to atoms. Phys. Rev. B, 18(10):5449–5472, Nov 1978.

[6] Steven G. Louie, Sverre Froyen, and Marvin L. Cohen. Nonlinear ionic pseudopotentials in spin-density-functional calculations. Phys. Rev. B, 26(4):1738–1742, Aug 1982.

[7] Vladimir I. Anisimov, Jan Zaanen, and Ole K. Andersen. Band theory and Mott insulators: Hubbard u instead of Stoner i. Phys. Rev. B, 44(3):943–954, Jul 1991.

[8] S. L. Dudarev, G. A. Botton, S. Y. Savrasov, C. J. Humphreys, and A. P. Sutton. Electron-energy-loss spectra and the structural stability of nickel oxide: An LSDA+U study. Phys. Rev. B, 57(3):1505–1509, Jan 1998.

[9] A. G. Petukhov, I. I. Mazin, L. Chionel, and A. I. Lichtenstein. Correlated metals and the LDA+U method. Phys. Rev. B, 67:153106, 2003.

[10] A. I. Liechtenstein, V. I. Anisimov, and J. Zaanen. Density-functional theory and strong interactions: Orbital ordering in Mott-Hubbard insulators. Phys. Rev. B, 52(8):R5467–R5470, Aug 1995.

[11] Deepa Kasinathan, Klaus Koepernik, and Warren E. Pickett. Pressure-driven magnetic moment collapse in the ground state of MnO. New J. Phys., 9:235, 2007.

[12] K.-W. Lee and W. E. Pickett. Infinite-layer $LaNiO_2$: Ni^{1+} is not Cu^{2+}. Phys. Rev.B, 70(16):165109, Oct 2004.

[13] V. I. Anisimov, I. V. Solovyev, M. A. Korotin, M. T. Czy˙zyk, and G. A. Sawatzky. Density-functional theory and NiO photoemission spectra. Phys. Rev. B, 48(23):16929–16934, Dec 1993.

[14] M. T. Czy˙zyk and G. A. Sawatzky. Local-density functional and on-site correlations: The electronic structure of La2CuO4 and LaCuO3. Phys. Rev. B, 49(20):14211–14228, May 1994.

CHAPTER 4

CALCULATION DETAILS

In this chapter, we firstly reviews the structure and details of the LMTART program, which is based on the DFT methods. We then discuss the MStudio program, the scientific software for windows systems, that performs the electronics of crystalline solids. Especially, the spin (m_s) and orbital (m_o) magnetic moment of antiferromagnetic NiO and MnO have been studied by MStudio program within the Coulomb interaction U varying from 0 to 10 eV, the exchange interaction J, from 0 to 1.0 eV and volume compression VC in range of 0 to 80%. We also explain the control files that need to be prepared for implementation of the MStudio.

4.1 Introduction

In this section, we briefly describe the control files that need to be prepared for the implementation of LMTART program. For LSDA calculations only, there are two essential input files - the *ini* and the *str* filles. The *ini* file contains details about the various approximation schemes such as `full-potential plane wave' or `atomic sphere approximation' as well as those about the exchange-correlation functional. It also contains information about the different atoms in the unit cell. The structure file or the *str* file has information about the crystal structure. In additional, For LSDA+U, we need the *hub* file that contains the interaction parameters. Each control file is divided into different sections, separated by <SECTION = >, each containing a certain set of data. There are certain common features in each control file:

The first line <FILE = ***FILE, INPUT = MODERN> where `***' stands for the type of control file - i.e., INI or STR or HUB, must be present in each control file. This line is required by the main program in the LMTART program to call the corresponding subroutine to read the control file. The first section in the control files contains the title of the material, that it is optional. A comment that usually contains the description of the parameter and some options for it can be placed on each line after a `!' mark. Many parameters have default values. If a default value exists, this parameter can be omitted from the file.

4.1.1 INI file

<SECTION = CTRL>

Parameters in this section control the choice of the scheme we would like to use in the implementation of LMTART.

- FullPot, This parameters allows us to choose the approximation for the potential seen by an atom in the solid. The choices are a Full Potential plane wave approximation (PLW) or the atomic sphere approximation (ASA) where the potential in the interstitial region is approximated by a constant.

<SECTION = ITER>

This section control the iterational loop

<SECTION = MAIN>

This section contains information about the number of atoms and spins in the unit cell.

- *Nsort* : The number of non-equivalent atoms in the unit cell. This parameter becomes important in anti-ferromagnetic calculations as explained in section 4.3.3.
- *Is* : This labels the different kinds of basis atoms. The order must correspond to that in <SECTION = BASS> in the *str* file. An example is provided in Table 4.1.
- *Par0* : The lattice parameter in atomic units needs to be provided, which is used, along with the crystal structure to calculate the energy in Rydberg units. 1 Ry = 13.605 eV.

<SECTION = SORT>

This section contains information about the atoms. Once the name and atomic number of each element is entered, the LMTART routine searches for relevant information for the atom in the directory /atomdat/. Set of parameters in <SECTION = SORT> must be entered for each non-equivalent atoms being indicate in the parameter Nsort.

Table 4.1 : *INI* File or Input file of ferromagnetic NiO , NiO.ini

```
<FILE=INIFILE,INPUT=MODERN,TRACE=FALSE>
*************************************************************************
 <SECTION=HEAD>                 ! PROJECT HEAD:
     title = nio                ! Compound title
 <SECTION=CTRL>                 ! CONTROL PARAMETERS:
     Lmto  =Bare                ! set: Bare / Screened / Rspace
     FulPot=ASA                 ! set: FTB/ ASA / PLW
 <SECTION=EXCH>                 ! EXCHANGE-CORRELATION:
     LDA   =Vosko               ! set: none/Barth/Gunn/etc.
<SECTION=ITER>                  ! ITERATIVE PROCEDURES:
     Niter1=50                  ! # of iterations in SCF loop
<SECTION=MAIN>                  ! MAIN ATOMIC DATA:
     Natom =2                   ! # of atoms in the unit cell
     Nsort =2                   ! # of sorts in the unit cell
     Nspin =1                   ! # of spins
     Norbs =1                   ! 1-wthout / 2 – with spin orbital coupling
     Par0  = 7.92600            ! lattice parameter in a.u.
     Is(:) =1 2                 ! atom-to-sort pointer array
<SECTION=SORT>                  ! SORT DATA:
     Name  = Ni1                ! atom label
     Znuc  = 28.0000            ! nuclear charge
     Smts  = 2.17900            ! non-overlapping MT-sphere
     Split = 0.50000            ! initial splitting
<SECTION=SORT>                  ! SORT DATA:
     Name  = O                  ! atom label
     Znuc  = 8.00000            ! nuclear charge
     Smts  = 1.78300            ! non-overlapping MT-sphere
     Split = 0.00000            ! initial splitting
<SECTION=FFTS>                  ! FFT GRIDS:
    Ndiv(:)=4 4 4               ! Tetrahedron mesh
```

4.1.2 STR file

The structure file contains all the information about the crystal structure. To prepare the file, we need to know about the unit cell of the lattice, -the parameters describing the geometry of the cell, the primitive translation vectors and the basis atoms. This information can be obtained from experimental values.

Table 4.2 describes a sample *str* fille for ferromagnetic NiO which has a fcc structure with two basis atoms, i.e. Ni and O. The unit cell for this is schematically shown in Figure 4.1. n the notation we use, the primitive vectors of the unit cell are expressed as $A\hat{x}+B\hat{y}+C\hat{z}$ as shown in Figure 4.1.

<SECTION = CTRS>

- *Natom*: The total number of basis atoms in the unit cell. For the above example of NiO it is 2. (no default)
- *B to A*: The ratio of the length along the y-direction to that along the x-direction. In the above example, we have a cubic cell, hence this ratio is 1. (default is 1.0)
- *C to A*: The ratio of the length along the z-direction to that along the x-direction. In the above example, we have a cubic cell, hence this ratio is 1. (default is 1.0)

<SECTION = TRAN> (no default)

This section contains the primitive translation vectors of the lattice. For example, for the fcc lattice the set of vectors can be written as $\left(\left(\frac{1}{2},\frac{1}{2},0\right),\left(0,\frac{1}{2},\frac{1}{2}\right),\left(\frac{1}{2},0,\frac{1}{2}\right)\right)$ and for the bcc lattice the set is $\left(\left(\frac{1}{2},\frac{1}{2},-\frac{1}{2}\right),\left(-\frac{1}{2},\frac{1}{2},\frac{1}{2}\right),\left(\frac{1}{2},-\frac{1}{2},\frac{1}{2}\right)\right)$

<SECTION = BASS> (no default)

This section contains the positions of the basis atoms in the unit cell, that along with the primitive translations from the above section will generate the full lattice. Note: The order in which the basis atoms are written mut correspond to the order in which the atoms are written in <SECTION = SORT> in the *ini* file.

Table 4.2 : *STR* File or Input file of ferromagnetic NiO , NiO.str

```
<FILE=STRFILE, INPUT=MODERN>
**********************************************************************
<SECTION=HEDS>                    ! STRUCTURE TITLE:
      Slabl =NiO
<SECTION=CTRS>                    ! CONTROL STRUCTURE:
      Natom = 2                   ! # of atoms
      BtoA  = 1.00000             ! b over a ratio
      CtoA  = 1.00000             ! c over a ratio
<SECTION=TRAN>                    ! PRIMITIVE TRANSLATIONS:
      1/2 , 1/2 , 1.0             ! Ax,Ay,Az
      1/2 , 1.0 , 1/2             ! Bx,By,Bz
      1.0 , 1/2 ,1/2              ! Cx,Cy,Cz
<SECTION=BASS>                    ! BASIS ATOMS :
      0.0 , 0.0 , 0.0             ! Ni@1
      1/2 , 1/2 , 1/2             ! O@2
```

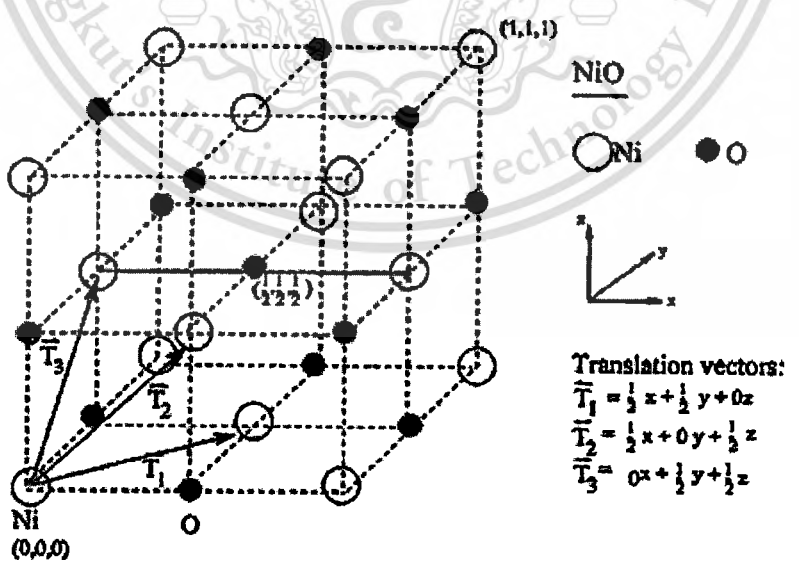

Figure 4.1 Unit cell for ferromagnetic NiO and translation vector.

4.1.3 Modifications for anti-ferromagnetic materials

If we need to compute the antiferromagnetic material for a given material, we need to make appropriate changes in the *ini* as well as *str* files. To have an antiferromagnetic, we pick alternate magnetic atoms in the lattice to have up and down spins respectively. The unit cell thus has to be doubled, and contains two non-identical magnetic atoms due to different spins, even though the atomic numbers of the two atoms remain the same.

The main modifications in the *ini* file are in <SECTION = MAIN> as shown in a part of the *ini* file for anti-ferromagnetic NiO in Table 4.3. Note, especially, the parameter Is(:) which sorts the different atoms. Even though Atom 1 and Atom 2 are both nickel, we treat them differently due to their different spins. <SECTION = SORT> contains information about the different spins in the parameter Split which has different signs for potential for up and down spins.

To determine the crystal structure we treat the lattice as a new structure with different primitive translations and basis atoms and re-construct the *str* file. For the same example of NiO as above, we begin with Figure 4.2 to generate the primitive translations and basis atoms. The *str* file for this case is shown in Table 4.4.

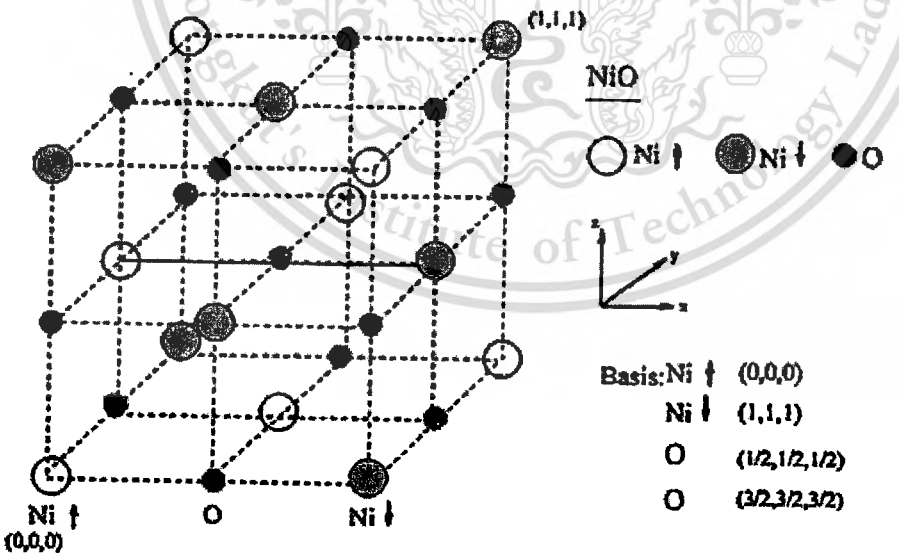

Figure 4.2 Unit cell for antiferromagnetic NiO and translation vector.

Table 4.3 : *INI* File or Input file of antiferromagnetic NiO , NiO.ini

```
<FILE=INIFILE,INPUT=MODERN,TRACE=FALSE>
**************************************************
<SECTION=MAIN>                  ! MAIN ATOMIC DATA:
    Natom = 4                   ! # of atoms in the unit cell
    Nsort = 3                   ! # of sorts in the unit cell
    Nspin = 2                   ! # of spins
    Norbs = 1                   ! 1-without / 2-with spin orbital coupling
    Par0  = 7.92600             ! lattice parameter in a.u.
    Is(:) =1 2 3 3              ! atom-to-sort pointer array
    Ovrl  = 1.50000             ! Maximum allowed overlap for ASA
<SECTION=SORT>                  ! SORT DATA:
    Name  = Ni1                 ! atom label
    Znuc  = 28.0000             ! nuclear charge
    Smts  = 2.17900             ! non-overlapping MT-sphere
    Split = 0.50000             ! initial splitting
<SECTION=SORT>                  ! SORT DATA:
    Name  = Ni2                 ! atom label
    Znuc  = 28.0000             ! nuclear charge
    Smts  = 2.17900             ! non-overlapping MT-sphere
    Split =-0.50000             ! initial splitting
<SECTION=SORT>                  ! SORT DATA:
    Name  = O                   ! atom label
    Znuc  = 8.00000             ! nuclear charge
    Smts  = 1.78300             ! non-overlapping MT-sphere
    Split = 0.00000             ! initial splitting
<SECTION=FFTS>                  ! FFT GRIDS:
    Ndiv(:)=4 4 4               ! Tetrahedron mesh
```

Table 4.4 : *STR* File or Input file of ferromagnetic NiO , NiO.str

```
<FILE=STRFILE, INPUT=MODERN>
**********************************************************************
<SECTION=HEDS>                  ! STRUCTURE TITLE:
    Slabl =NiO
<SECTION=CTRS>                  ! CONTROL STRUCTURE:
    Natom =4                    ! # of atoms
    BtoA  = 1.00000             ! b over a ratio
    CtoA  = 1.00000             ! c over a ratio
<SECTION=TRAN>                  ! PRIMITIVE TRANSLATIONS:
    1/2 , 1/2 , 1.0             ! Ax,Ay,Az
    1/2 , 1.0 , 1/2             ! Bx,By,Bz
    1.0 , 1/2 , 1.2             ! Cx,Cy,Cz
<SECTION=BASS>                  ! BASIS ATOMS :
    0.0 , 0.0 , 0.0             ! Ni@1
    1.0 , 1.0 , 1.0             ! Ni@2
    1/2 , 1/2 , 1/2             ! O@3
    3/2 , 3/2 , 3/2             ! O@4
```

4.1.4 HUB file

The main data in this file that need to be entered by the user are the choice of scheme to treat the correlated orbitals (LDA+U or LDA+DMFT) and the values of the interaction parameters. After the first iteration, additional data regarding occupancy matrices, self-energies and potential terms are written into this file.

A sample *hub* file for the antiferromagnetic case in NiO is shown in Table 4.5. All the energy values are in Rybergs. The various sections are explained below:

<SECTION = CTRL>

- Scheme : The details about the scheme to be used to treat the correlated orbitals, i.e. LDA+U or LDA+DMFT. A list of all the possible schemes that can be used is present in the file *hub_readhub.f* and *hub_ hubpot.f.*
- Ncrl : The number of states which appear in the correlated term. Descriptions and options of the other parameters in this section appear as comments in the hub file in Table 4.5.

<SECTION = CORR>

This section has the core information about the interaction terms.

- Cstate : This points to the atom that has correlations, its position in <SECTION = BASS > in the *str* file and the correlated orbital.
- *F0, F2, F4, F6* : These are parameters that appear in the Slater integrals. For *d*-electrons, three constants *F0, F2* and *F4* are needed and for *f*-electrons, there are four constants *F0, F2, F4* and *F6*. These can be linked to U and J via $U = F0$ and $J=(F2+F4)/14$ for d-electrons with $F2/F4 \simeq 0.625$. For *f*-electrons, $U = F0$ and $J=\frac{286F2+194F4+250F6}{6435}$

<SECTION = DHUB>

From this section onwards, data about occupancy matrices, self-energies etc are written into the *hub* file after the first iteration. These quantities are self-consistently calculated at each iteration and are rewritten.

Table 4.5 : *HUB* File or Input file of ferromagnetic NiO , NiO.hub

```
<FILE=HUBFILE,INPUT=MODERN,TRACE=TRUE>
**************************************************
 <SECTION=CTRL>                    ! CONTROL PARAMETERS:
      Scheme=LDA+U                 ! LDA/LDA+U
      Yharm =cubic                 ! Cubic/Spherical harmonics (output)
      Iharm =cubic                 ! Cubic/Spherical harmonics (input)
      Rorbs =One                   ! One/Both orbits to read
      Rspin =Both                  ! One/Both spins  to read
      Format=complex               ! Real/Complex input/output
      Ncrl  =  2                   ! # of correlated states
<SECTION=CORR>                     ! CORRELATED STATES:
      Cstate  =Ni1@1::3d           ! Correlated state pointer
      F0 = 0.5880000               ! Slater integrals
      F2 = 0.6012300               ! Slater integrals
      F4 = 0.3787700               ! Slater integrals
<SECTION=CORR>                     ! CORRELATED STATES:
      Cstate  =Ni1@2::3d           ! Correlated state pointer
      F0 = 0.5880000               ! Slater integrals
      F2 = 0.6012300               ! Slater integrals
      F4 = 0.3787700               ! Slater integrals
<SECTION=DHUB>                     ! PARTIAL OCCUPANCIES:
     cState=Ni1@1::3d              ! spin up/dn-up/dn data are :
        yz          zx          xy          x2-y2       3z2-1      REAL,Up-Up
     0.9540211   0.0000329   0.0000329  -0.0005166   0.0002983      yz
     0.0000329   0.9540211   0.0000329   0.0005166   0.0002983      zx
     0.0000329   0.0000329   0.9540211   0.0000000  -0.0005966      xy
    -0.0005166   0.0005166   0.0000000   0.1318555   0.0000000      x2-y2
     0.0002983   0.0002983  -0.0005966   0.0000000   0.1318555      3z2-1
```

4.2 Setting the MStudio Program

In this section, we describe a basic features and setting the MStdio program to calculate an electronic structure and the magnetic properties of NiO and MnO under a different condition as Coulomb interaction U, exchange interaction J and volume compression VC.

4.2.1 Overview of MStudio

MStudio, the scientific software for windows systems, represents a framework which controls several windows operating libraries such as BandLab Library and MScene Library dynamically linked with MStudio. The BandLab Library is designed to perform electronic structure calculations of the materials and compute physical properties of solids. BandLab also uses MScene library for visualization. Figure 4.3 show feature of MStudio program.

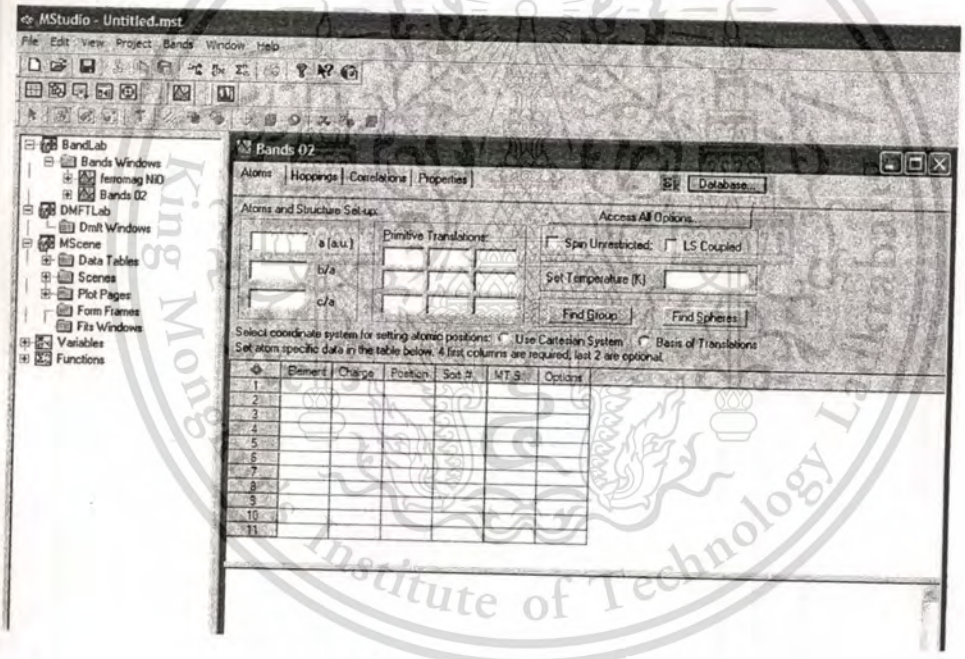

Figure 4.3 MStudio program

BandLab, as shown in Figure 4.4, consists of a window that is used to set up input data, perform calculations and analyze output data. The BandLab Window, shortly Bands Window is called using Bands command of the *Project menu* or corresponding button of the *Bands* Toolbar. The Bands window consists of *Atoms Page, Hoppings Page, Hubbards Page and Properties Page.*

The BandLab has a database of compounds that have been calculated using the LmtART program. The database is an important part of the library, it can be called by pressing DataBase button located on the top right part of the Bands Window. The input/output files can be stored within the database.

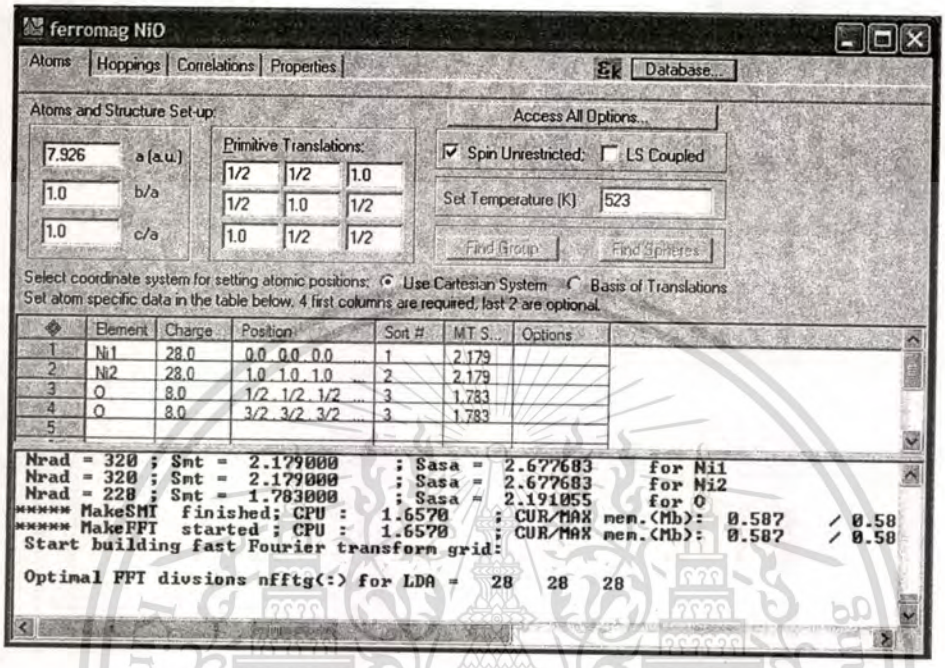

Figure 4.4 The BandLab Window

The BandLab is a program called LmtART. The LmtART is an executable file that reads the input data, performs band structure calculation, and stores the output files. The Bands Window only controls this process, it prepares input for the LmtART using dialog windows, and starts LmtART program as a separate thread. When the calculation is finished, LmtART notifies the BandLab, and the output files are read by the Bands Window and can be visualized by MScene.

4.2.2 Setting Atomic Data

Figure 4.5 shows atomic data set-up is the primary set of data describing the crystalline solid. The first property page of the Bands Window is designed to describe these parameters: Lattice parameter in atomic units, b/a and c/a ratios if the lattice has orthorhombic distortions, primitive translations in units of lattice parameter, spin polarization or spin-orbit coupling and temperature.

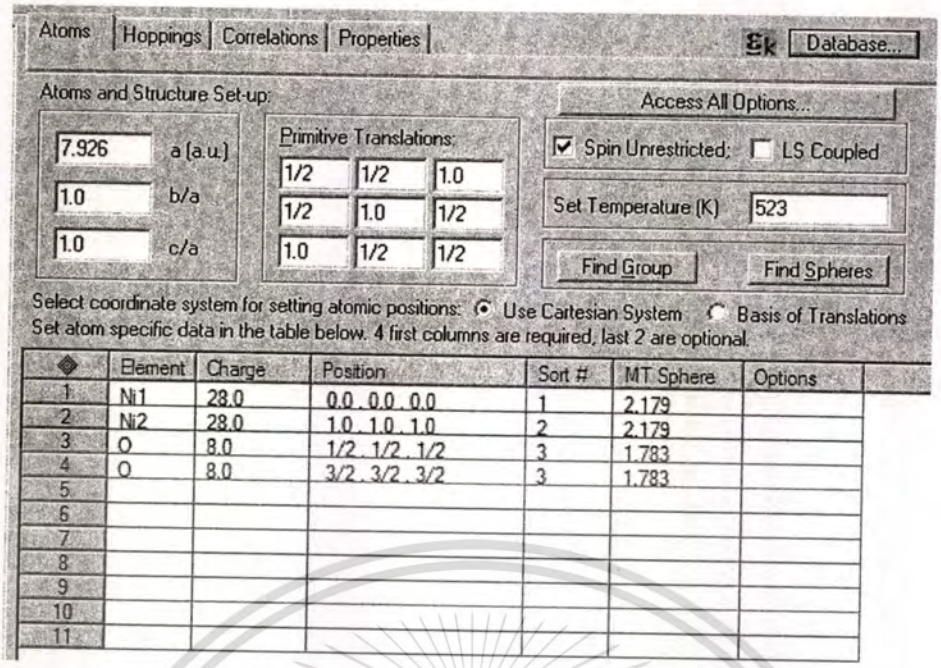

	Element	Charge	Position	Sort #	MT Sphere	Options
1	Ni1	28.0	0.0 0.0 0.0	1	2.179	
2	Ni2	28.0	1.0 1.0 1.0	2	2.179	
3	O	8.0	1/2 1/2 1/2	3	1.783	
4	O	8.0	3/2 3/2 3/2	3	1.783	
5						
6						
7						
8						
9						
10						
11						

Figure 4.5 Atomic data set-up

Structural parameters have to be described using this property page. Lattice parameter should be given in atomic units (a.u.), that 1 a.u. = 0.0529 nm. *b/a* and *c/a* ratios set scaling of y and z components for primitive translations.

The following set of data has to be given for each atom in the unit cell

- *Element title* such as Ni, O, Si, N etc.
- *Nuclear charge* is the most important parameter which the software recognizes the atoms.
- *Position* of atom in the unit cell in the units of lattice parameter.
- *If several atoms* have the same type, specify it in the Sort column. This will be used to determine crystal group. For example, the compound NiO has 4 atoms. At the same time there only 3 nonequivalent atoms: Ni1, Ni2, and 2*O. Therefore, sort column will be 1 for Ni@1, 2 for Ni@2, 3 for O@3, 3 for O@4. Here El@N shortly denotes the element at position N.
- *The radius* of the MT sphere can be optionally specified if this value is known. If this value is unknown, it can be computed by the LmtART.

4.2.3 Setting Correlations or Setting U and J Parameter

Correlations among *d*- or *f*- electrons in solids are important for determining their physical properties. Local density approximation (LDA) and generalized gradient approximations (GGA) do not treat properly systems with the correlated electrons. BandLab currently offers LDA+U scheme for including the effects of strong correlations into account. way of operating with these problems. The properties for the correlated orbitals can be accessed via calling Properties Dialog Box as shown in Figure 4.6 .

The following inputs are required to set up correlations:

- Basis set for correlated orbitals

  El@N::*nl* with *El* is an element title, *N* is the position number,

  n is the main quantum number and *l* is the orbital quantum number

  For example Ni 3d orbitals are represented by Ni@1::3d and Ni@2::3d.

- Slater integrals should be specified in the Options column.

  For *d*-electrons these are *F0, F2,* and *F4* parameters.

  $U = F0$, $J = (F2+F4)/14$ Ryberge unit , which 1 Ry = 13.605 eV.

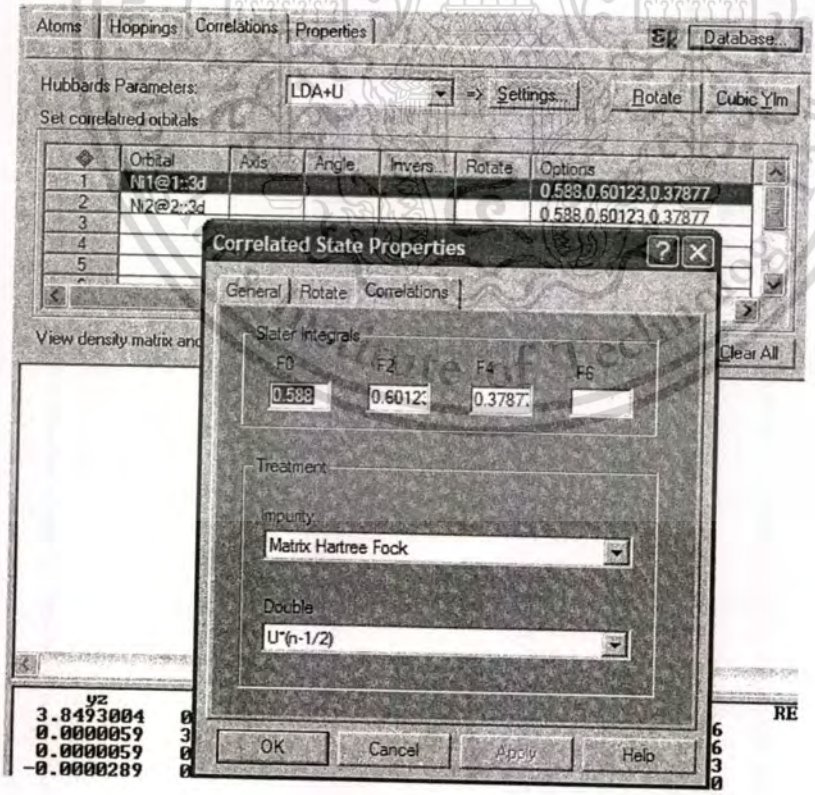

Figure 4.6 setting Correlations box

4.2.4 Setting Volume Compression

If volume compression of the lattice is required, change only the parameter V/V0. Do not change lattice constants, sphere radii and any other data. Figure 4.7 show the setting volume is compressed 10% by volume.

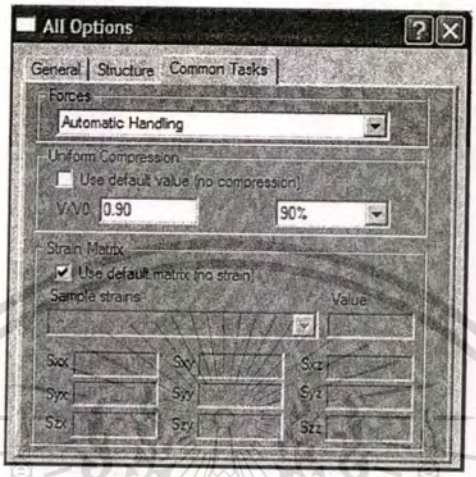

Figure 4.7 setting volume compression

4.2.5 Setting magnetic properties of an atom

To find the magnetic spin ordered solutions, the quantization axis and initial magnetic field can be given. Without spin orbit coupling effects, the quantization axis is always assumed along z direction. If spin orbit coupling is switched on, the quantization axis can align along any direction. The initial magnetic field will be switched on along magnetization axis to kick the atom out of the paramagnetic state.

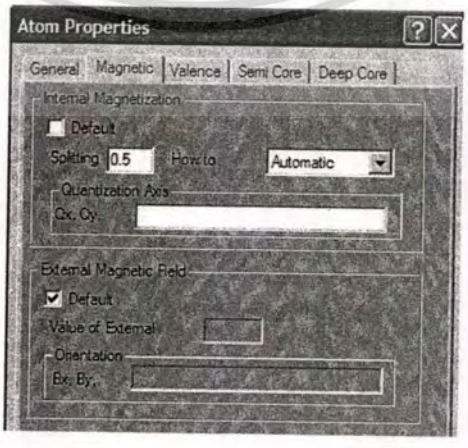

Figure 4.8 Setting magnetic properties of atom

4.3 Computing Physical Properties and Visualization

Computation of physical properties is the goal of the BandLab library. The LmtART program is the executable module that does this calculation. It reads input files prepared by the bands Window, performs the calculation of the desired property, and notifies the Bands Window again that the calculation is finished. The BandLab reads the output files and visualizes them with help of the MScene library.

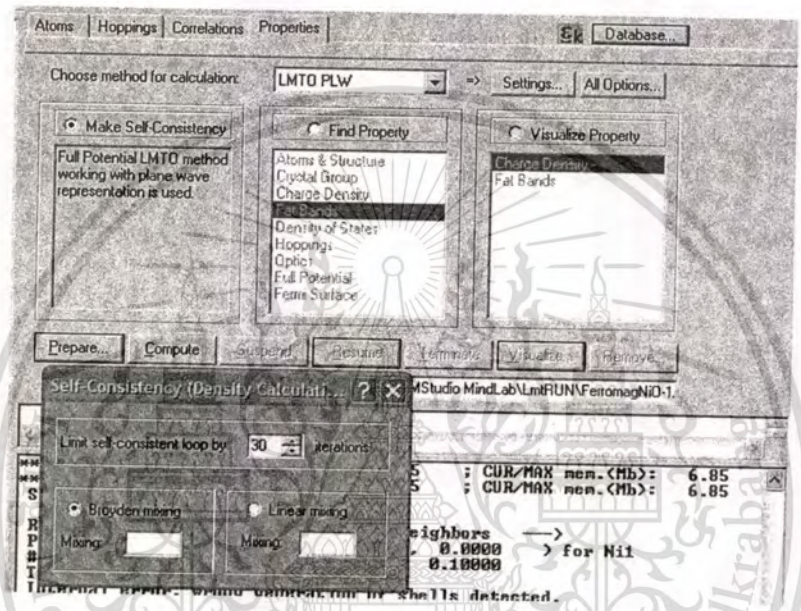

Figure 4.9 Computing Physical Properties and Visualization

Choose method for calculation

- Full potential LMTO method for electronic structure calculation. This is the most precise approach for computing physical properties such as one-electron structure, but at the same time, it is computationally slow approach.
- ASA-LMTO method for electronic structure calculation. This is a fast method, but less accurate comparing to the full potential LMTO method.

Both FP-LMTO and ASA LMTO methods require self-consistent calculation to be performed before computing any physical property such as the band structure or density of states. To make self-consistency, switch on radio button *Make Self-Consistency* and click *Compute* button. The self-consistent calculation will start. The output window in the lower part of the Bands Window will show

how the self-consistent process is performed. However maybe rather slow process especially when compounds with many atoms are considered. At the end of the calculation, the framework creates the file consisting the self-consisting charge density.

To compute physical property such as Fat Bands, set radio button *Find Property* to the On position. Chose *Fat Bands property* from the drop-down list and press Compute button. The following set of properties can be computed by the BandLab: *Atoms & Structure,Crystal Group, Charge Density, Fat Bands, Density of States, Hoppings, Optics, Full Potential and Fermi Surface*

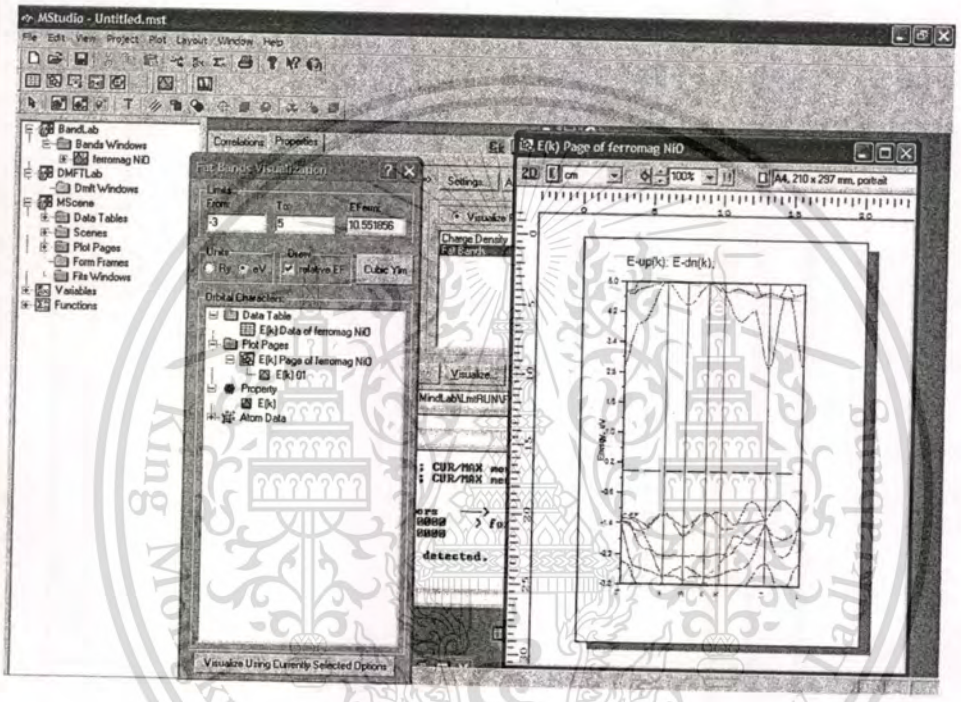

Figure 4.10 Fat Bands of NiO within $U = 5.8$ eV and $J = 0.98$ eV.

```
Input/output magnetic moment at the iteration
    M(inp)              M(out)
 -1.806410           -1.806414      for Ni1
  1.806410            1.806414      for Ni2
-0.6661338E-14        0.000000      for O
-0.5329071E-14        0.000000      for O
    I(inp)              I(out)
  3.597027            3.597026
  3.597026            3.597026
```

Figure 4.11 Magnetic moment of NiO within $U = 5.8$ eV and $J = 0.98$ eV and self-consistent SCF 30 loop.

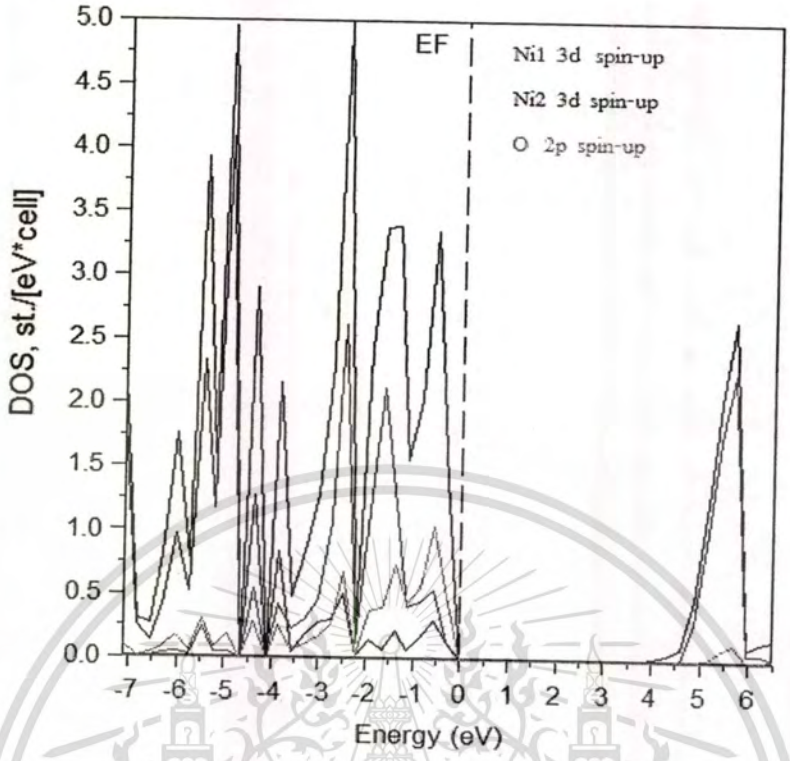

Figure 4.12 DOS (black) and PDOS (color) of NiO within $U = 5.8$ eV and $J = 0.98$ eV.

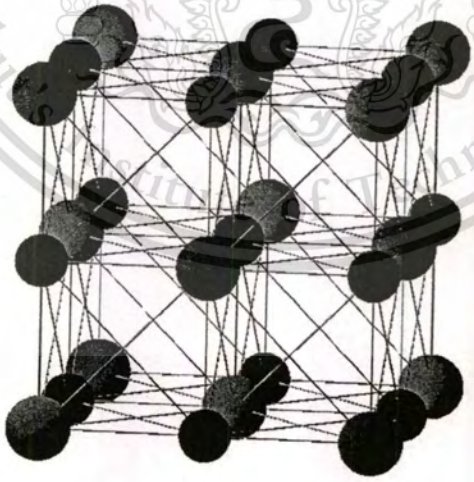

Figure 4.13 Atomic and structure of antiferromagnetic type II - NiO ,Ni-spin up (red sphere), Ni-spin down (green sphere) and O-ion (blue sphere)

4.4 Preparing Control Files for AFM II -NiO

Our calculations assumed NiO as a type II antiferromagnetic (AFM II) with lattice constant *a* of 0.419nm (7.926 a.u.). The muffin-tin radii of Ni^{2+} and O^{2-} ions are 2.179 and 1.783 a.u, respectively and the volume compression was defined by *V/Vo* ratio. The effect of *U, J* and VC on spin and orbital magnetic moments of NiO were studied by varying *parameter U, J* and VC ranging from 0-10 eV, 0 – 1.0 eV and 0-80%, respectively.

4.4.1 Setting atoms and structure of NiO

Figure 4.13 show a setting atoms and structural parameter of NiO. Lattice constant should be given in atomic units (a.u.) , which 1 a.u. = 0.0529nm., while b/a and c/a ratios set scaling of y and z components for primitive translations. The primitive translation vectors of lattice can be written as $\left(\left(\frac{1}{2},\frac{1}{2},1.0\right),\left(\frac{1}{2},1.0,\frac{1}{2}\right),\left(1.0,\frac{1}{2},\frac{1}{2}\right)\right)$. Spin–orbital coupling and temperature were defined.

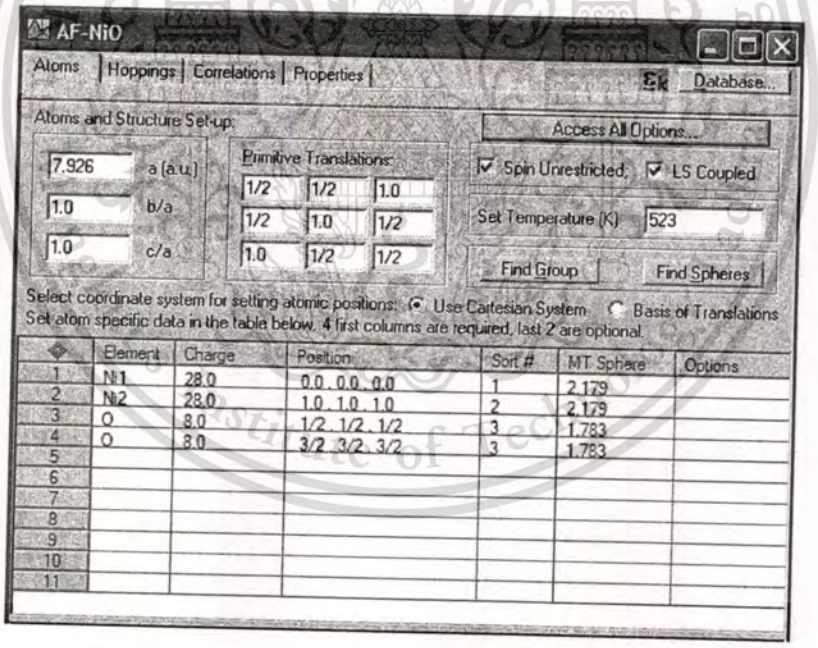

Figure 4.14 . Setting atoms and structure of antiferromagnetic type II NiO

The following of data has to be given for each atom in the unit cell

- Element title : Ni1, Ni2 and O represent Nickel atom and Oxygen atom , respectively.
- Nuclear charge is the most importance parameter which, for Ni = 28 and O = 8
- position of atom in unit cell. Sort columm is nonequivalent atom in unit cell.

4.4.2 Setting parameter U and J on NiO

The properties for the correlated orbitals can be accessed via calling properties dialog box as shown in Figure 4.15. The following inputs are required to set up correlations

- Basis set for correlation orbitals : Ni 3d orbital are represented by Ni@1::3d and Ni@2 ::3d
- Slater integrals should be specified in the option columm. For *d*-electron these are *F0, F2* and *F4* parameter, which $U = F0$ and $J = \frac{F2+F4}{14}$, $\frac{F2}{F4} \approx 0.625$ Ry unit (Ryberge unit) and 1 Ry = 3.605 eV.

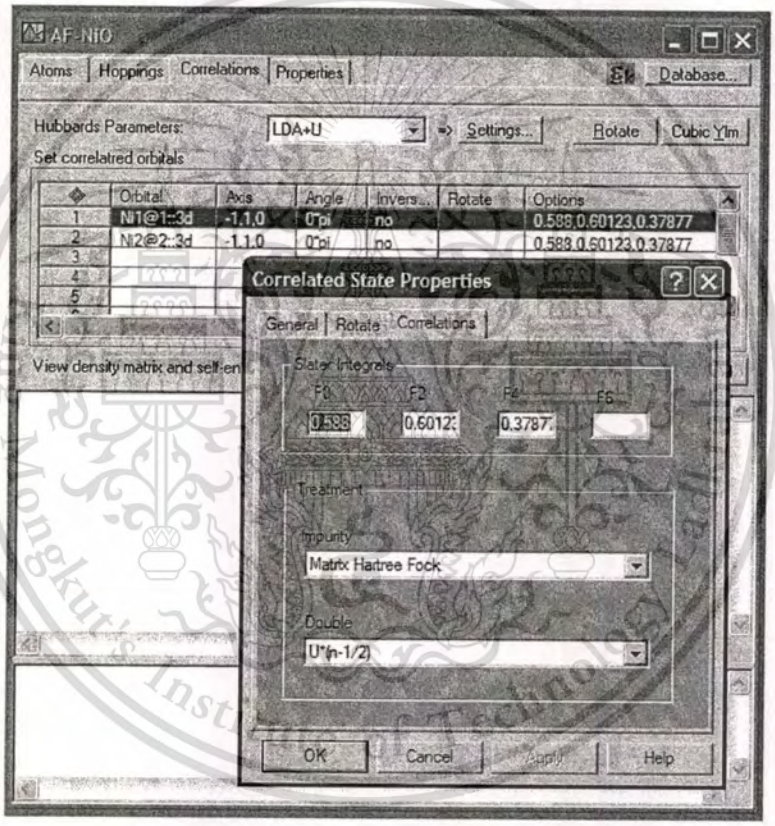

Figure 4.15 Setting U and J parameter of NiO

Table 4. 6 The values of Coulomb interaction U (eV) and the Slater integrals *F0* (Ry)

U(eV)	1.0	2.0	3.0	4.0	5.0	6.0	7.0	8.0	9.0	10
F0(Ry)	0.0735	0.1470	0.2205	0.2940	0.3675	0.4410	0.5145	0.5880	0.6615	0.7350

Table 4. 7 The values of exchange interaction J (eV) and the Slater integrals $F2$ and $F4$ (Ry)

J (eV)	*F2(Ry)*	*F4(Ry)*
0.10	0.06333	0.03958
0.20	0.12665	0.07916
0.30	0.18998	0.11873
0.40	0.25330	0.15831
0.50	0.31663	0.19789
0.60	0.37995	0.23747
0.70	0.44328	0.27705
0.80	0.50660	0.31663
0.90	0.56993	0.35620
1.00	0.63325	0.39578

4.4.3 Setting volume compression on NiO

The volume of unit cell were compressed by changing only parameter *V/V0* as shown in Figure 4.16. Do not change lattice constants, sphere radii and other data.

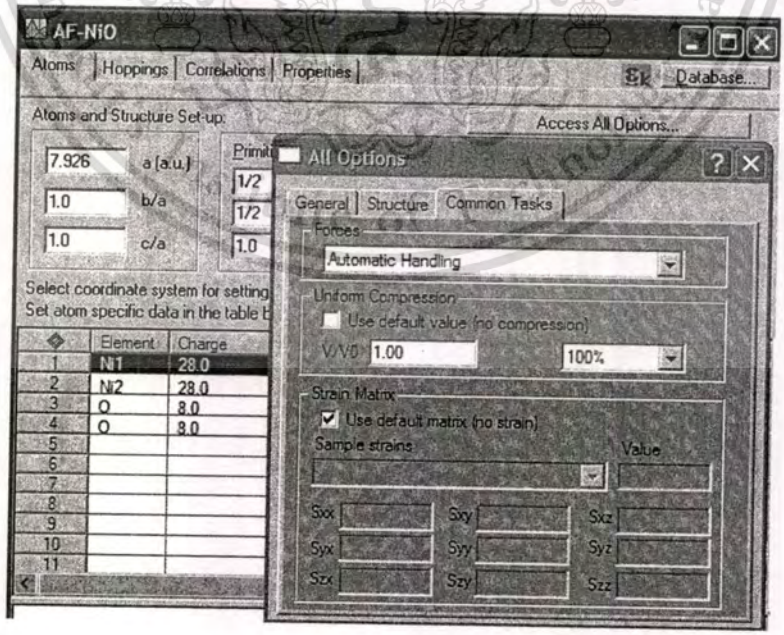

Figure 4.16 Setting volume compression of NiO

4.5 Preparing Control Files for AFM II -MnO

Our calculations assumed MnO as a type II antiferromagnetic (AFM II) with lattice constant *a* of 0.444nm (8.393 a.u.). The muffin-tin radii of Ni^{2+} and O^{2-} ions are 2.346 and 1.843 a.u, respectively and the volume compression was defined by *V/Vo* ratio. The effect of *U, J* and VC on spin and orbital magnetic moments of MnO were studied by varying *parameter U, J* and VC ranging from 0-10 eV, 0 – 1.0 eV and 0-80%, respectively.

4.5.1 Setting atoms and structure of MnO

Figure 4.17 show a setting atoms and structural parameter of MnO. Lattice constant should be given in atomic units (a.u.) , which 1 a.u. = 0.0529nm., while b/a and c/a ratios set scaling of y and z components for primitive translations. The primitive translation vectors of lattice can be written as $\left(\left(\frac{1}{2},\frac{1}{2},1.0\right),\left(\frac{1}{2},1.0,\frac{1}{2}\right),\left(1.0,\frac{1}{2},\frac{1}{2}\right)\right)$. Spin–orbital coupling and temperature were defined.

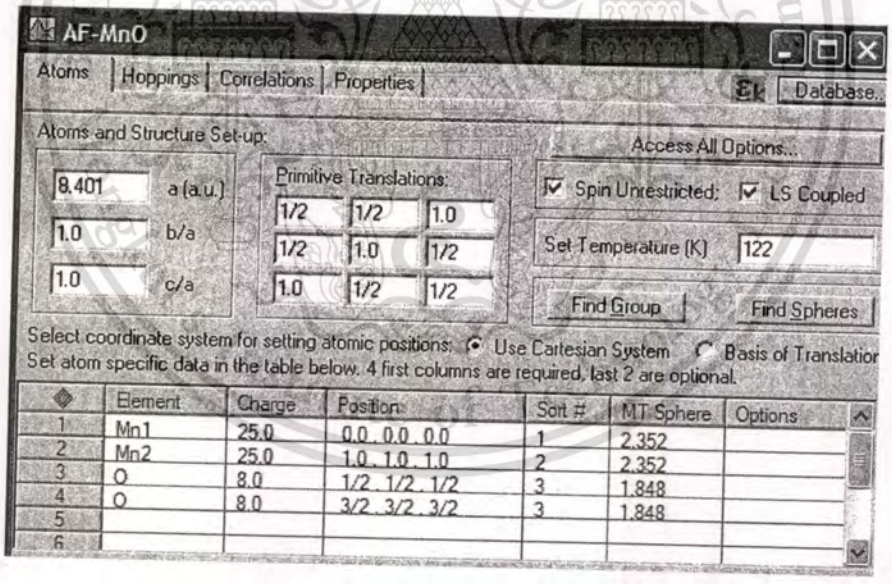

Figure 4.17 . Setting atoms and structure of antiferromagnetic type II MnO

The following of data has to be given for each atom in the unit cell

- Element title : Mn1, Mn2 and O represent maganese atom and oxygen atom , respectively.
- Nuclear charge is the most importance parameter which, for Mn = 25 and O = 8
- position of atom in unit cell. Sort columm is nonequivalent atom in unit cell.

4.5.2 Setting parameter U and J on MnO

The properties for the correlated orbitals can be accessed via calling properties dialog box as shown in Figure 4.18. The following inputs are required to set up correlations : Basis set for correlation orbitals : Mn 3d orbital are represented by Mn@1 ::3d and Mn@2 ::3d . Slater integrals should be specified in the option columm. For *d*-electron these are *F0, F2* and F4 parameter, which $U = F0$ and $J = \frac{F2+F4}{14}$, $\frac{F2}{F4} \approx 0.625$ Ry. (Ry= Ryberge unit, 1 Ry = 3.605 eV.)

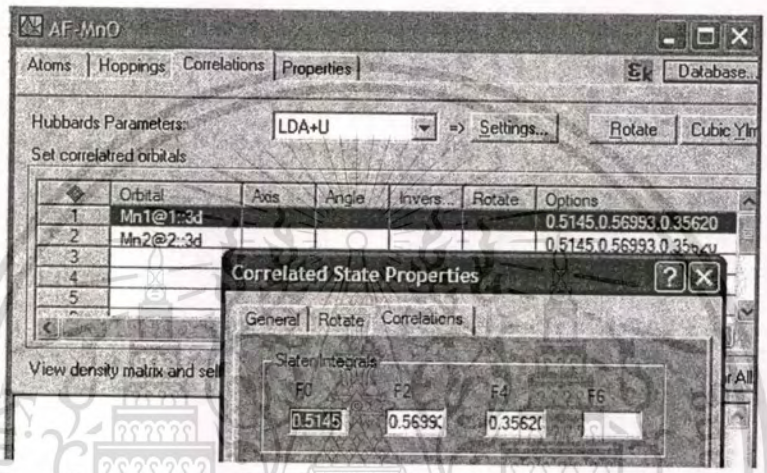

Figure 4.18 Setting U and J parameter of MnO

4.5.3 Setting volume compression on MnO

The volume of unit cell were compressed by changing only parameter *V/V0* as shown in Figure 4.19. Do not change lattice constants, sphere radii and other data.

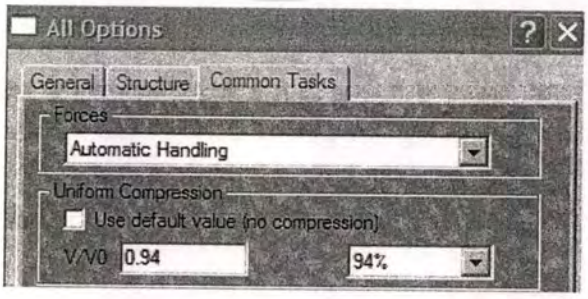

Figure 4.19 Setting volume compression of MnO

CHAPTER 5

RESULTS AND DISCUSSIONS

In this chapter, we reported the effect of Coulomb interaction U, the exchange interaction J and the volume compression VC on both spin and orbital magnetic moment. Our calculated results indicated that both spin (m_s) and orbital (m_o) magnetic moments strongly correlated to U, J and VC. The interesting behavior appears when volume compression is greater than 70% for NiO and 50% for MnO, at which m_s collapses.

5.1 Effect of the Coulomb interaction U on magnetic properties of NiO

Magnetic moments of NiO were evaluated as function of Coulomb interaction U and the corresponding result is illustrated in Figure 5.1. The calculation was carried out by the LSDA+U method at designated VC of 0, 20% and 40% and the exchanged interaction J = 0.95eV. The result shows that both spin and orbital magnetic moments gradually increase with increasing Coulomb interaction. This feature is understandable in view of the reason that Coulomb interaction U enhances the electron localization, which leads to magnetic moment gain. At the Coulomb interaction U of 6.0 eV and normal volume without compression, the spin and orbital magnetic moments m_s=1.80 μ_B and m_o=0.16 μ_B were obtained. Both spin and orbital magnetic moments of NiO were larger than in fcc Ni, which has m_s=0.63 μ_B and m_o=0.06 μ_B. This behavior suggests that 3d-electrons of NiO are likely localized in Ni metal [1].

Furthermore, The relation of magnetic moments and Coulomb interaction could be expressed as $m_s = 0.03U + 1.60\ \mu_B$ and $m_o = 0.003U + 0.14\ \mu_B$. The 10 % change of U can induce the change of about 0.3% and 0.03% in spin and orbital magnetic moments, respectively. Calculated magnetic moments were summarized in Table. 5.1 in comparison with experimental data and previous results by other calculated methods. Our calculated results reveal that the orbital magnetic moments are underestimated comparing to the experiment results [2] meanwhile the spin magnetic moment and Coulomb U values are agreement with experimental data [3, 4]. Figure 5.1 exhibits both spin and orbital magnetic moment depend strongly on the Coulomb interaction U in the range of 0 to 10 eV. The spin and orbital magnetic moment gradually increased to 1.87 μ_B and 0.17 μ_B, respectively, as shown in Table 5.1.

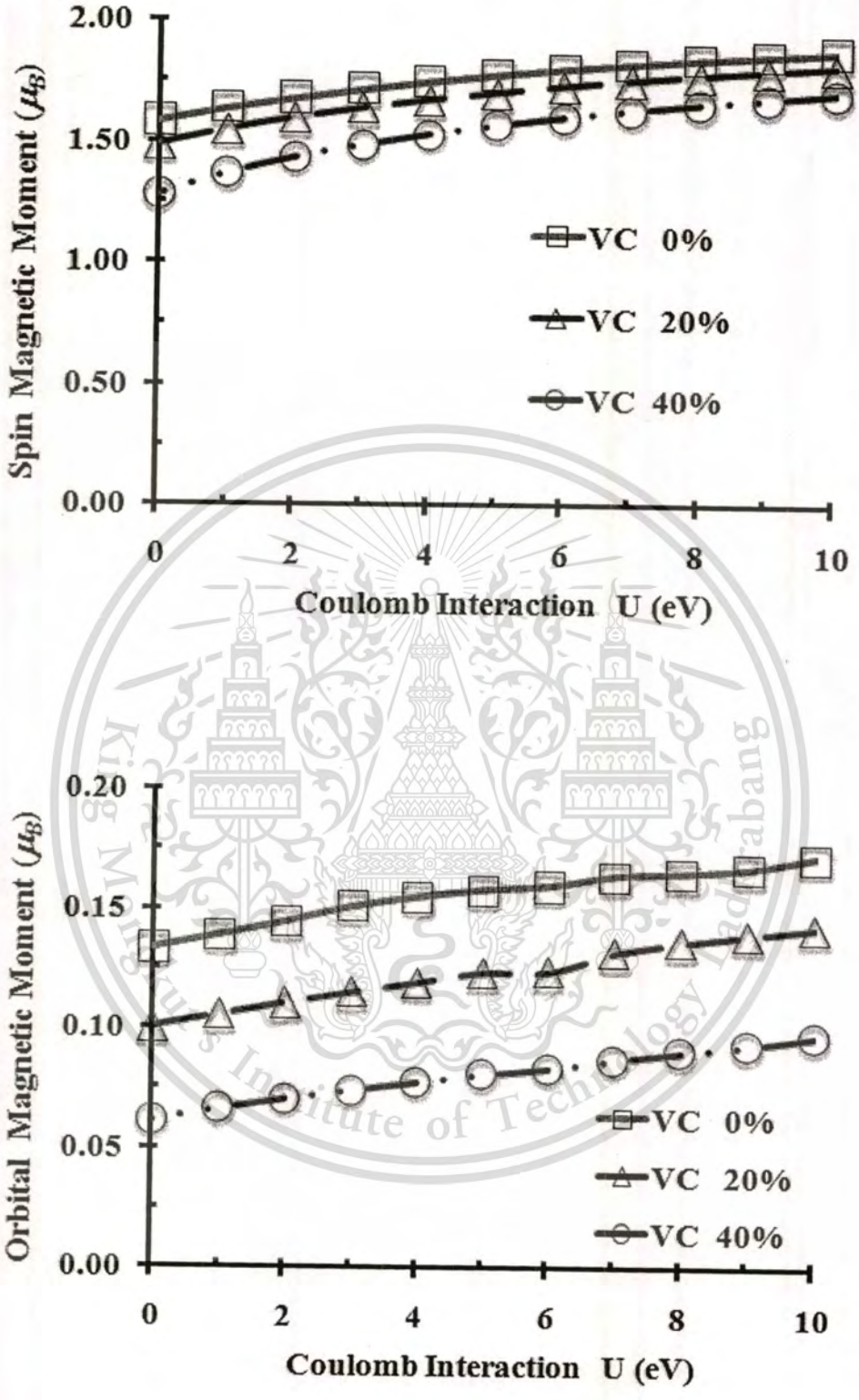

Figure 5.1 The variation of spin (top) and orbital (bottom) magnetic moment of NiO with Coulomb interaction *U*. (*VC* = 0, 20 and 40%)

Table 5.1 The values of spin and orbital magnetic moment of NiO at normal pressure, Coulomb interaction U, the exchange interaction J, were obtained from experiment and calculated methods.

Normal Pressure	Coulomb interaction U (eV)	Exchange interaction J (eV)	Spin magnetic moment (μ_B)	Orbital magnetic moment (μ_B)
Our Calculated Results [WC method]	1.0	0.95	1.64	0.14
	5.0		1.77	0.16
	6.0		1.80	0.16
	10.0		1.87	0.17
Experimental Data	5.8 [5]	-	1.64 [5] 1.77 [7] 1.90 [8]	0.32 [2]
QPs [6]	3.0	-	1.5	-
EXX [7]	-	-	1.89	-
GGA+U [1]	6.2	1.36	2.0	-
Crystal-field [8]	-	-	1.99	0.46
LDA+U^{d+p} [18]	8.0	0.95	1.64	-
LSDA+U [1]	8.0	0.89	1.64	0.29

5.2 Effect of the exchange interaction J on magnetic properties of NiO

Figure 5.2 shows the spin (m_s) and orbital (m_o) magnetic moment of NiO slightly increased with increasing of J since the exchange interactions should be analyzed by quantum theory, so it strongly concerns with spin-spin interactions. More specifically, on the atomic scale, the exchange interaction J tends to align neighbor spins so the spin magnetic moment increase with increasing of J. Relation of the magnetic moments and J could be expressed as $m_s = 0.10J + 1.67\ \mu_B$ and $m_o = 0.02J + 0.16\ \mu_B$.

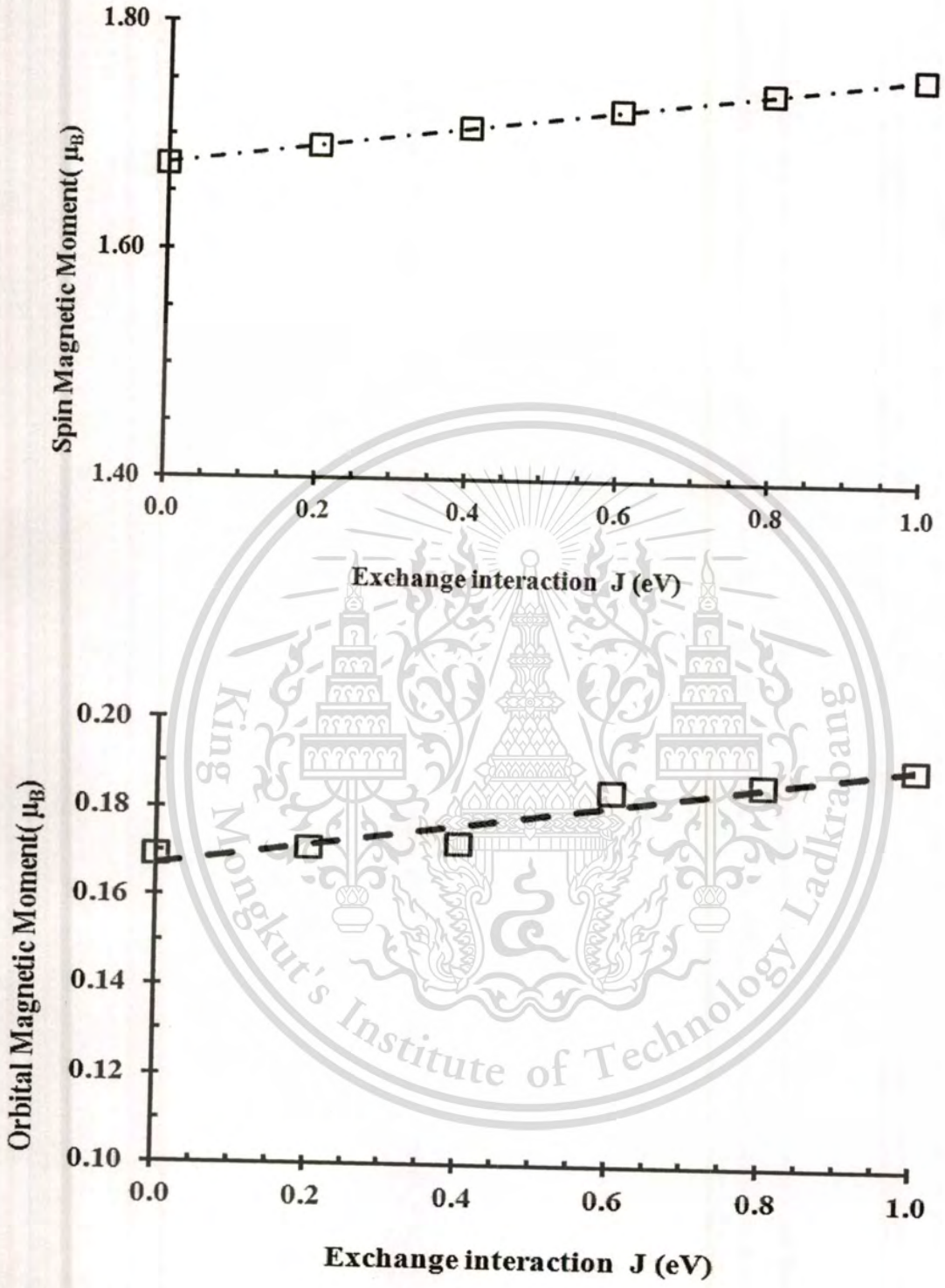

Figure 5.2 The variation of spin (top) and orbital (bottom) magnetic moment of NiO with the exchange interaction J, $U = 6.0\ eV$.

5.3 Effect of the volume compression *VC* on magnetic properties of NiO

Figure 5.3 shows the variations of the spin (m_s) and orbital (m_o) magnetic moments as a function of volume compression at various Coulomb interaction of 6, 8 and 10 eV. It is noticed that m_s and m_o decrease with increasing *VC* whereas the spin magnetic moment slightly decrease. At the compression range of 0 - 30%, the m_s decreases from its original value by 0.4% as the *VC* increases by 10%. Further increasing of *VC* by 40 -70 % results to the ~ 2% decrease of m_s for every 10% increasing *VC*. As the volume compression is larger than 70%, the spin magnetic moment rapidly decreases to zero. Meanwhile, the value of orbital magnetic moment gradually decreases by 2% for every 10% increasing *VC* until the collapse of m_o occurs at 80% of *VC*. This strange behavior may be originated from the delocalization of most electrons in NiO. The calculated results at room temperature with U = 6.0 eV gave the total magnetic moment $1.96\,\mu_B$ ($m_s = 1.80\,\mu_B$ and $m_o = 0.16\,\mu_B$). The calculated results of total magnetic moment (m_t) obtained by this present work and by Z. Ropka et. Al [9] are summarized and compared to the experimental data in Table 5.1. The theoretical spin magnetic moment extracted from our proposed model at U = 1.0 and 5.0 eV exhibits the closer agreement to experimental data than the other previous works [4, 5, 10].

In addition, in order to predict magnetic behavior of NiO under high pressure and obtain the transition pressure, the calculations were carried out for different unit cell volumes. The transition pressure was obtained by the thermodynamics equation, $P = -\partial E / \partial V$. Where *P*, *E* and *V* represent pressure, energy and volume, respectively. The comparison of the experimental volume compression data [5] and the theoretical results obtained at U = 6.0 eV is presented in Figure 5.4. As the pressure raises from normal pressure to 150 GPa, it is obviously noticed that the volume decreases from 0 to 30% and the lattice constant decreases from 4.19 Å to 3.72 Å, respectively. These significant decreases could consequently affect to the decrease in spin and orbital magnetic moment from $1.78\,\mu_B$ to $1.65\,\mu_B$ and $0.16\,\mu_B$ to $0.10\,\mu_B$ respectively. Based on our calculation, the disappearance of spin and orbital magnetic moment occurs at very high pressure in the vicinity of 5 TPa. This strange phenomena are quite interesting and still in doubt therefore the further deep researches not only experimental but also theoretical works are required for better clarification.

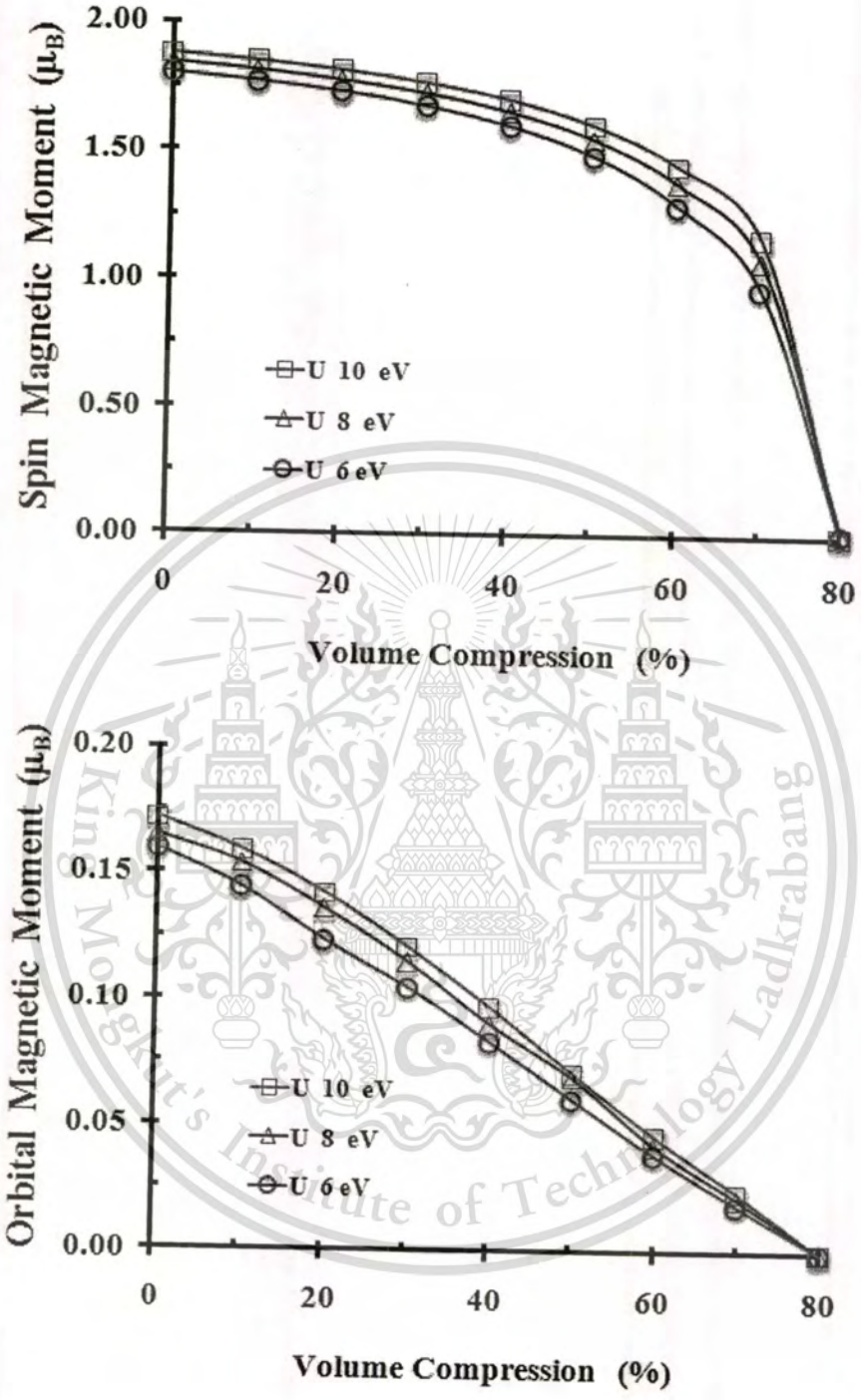

Figure 5.3 Spin (top) and orbital (bottom) magnetic moment depend on the volume compression. (U= 6, 8 and 10eV).

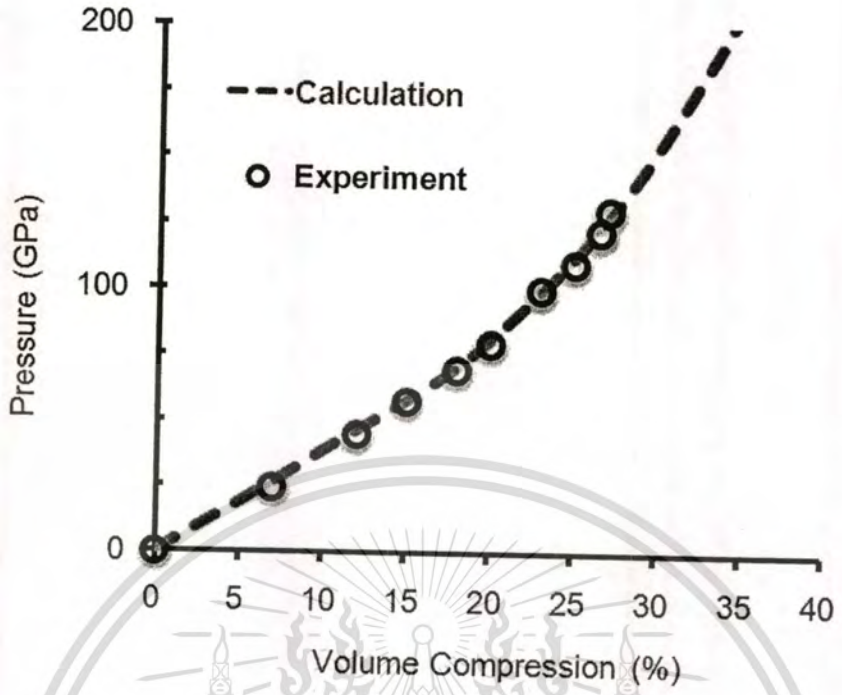

Figure 5.4 The variation of the pressure (GPa) with the volume compression (%). The solid dash lines and open circles represent to the calculation and the experimental result [11] respectively.

5.4 Effect of the Coulomb interaction U on magnetic properties of MnO

Our calculated results showed the spin magnetic moment as a function of Coulomb interaction U and exchange interaction J. In Figure 5.5 shows the spin magnetic moments were proportional to the Coulomb interaction U. This feature is understandable in view of the reason that the Coulomb interaction U enhances the electron localization, which leads to magnetic moment gain. The 10% change of U can induce the change of 0.2% in spin magnetic moment. Relation of the spin magnetic moment (m_s) and U could be express as $m_s = 0.02U + 4.55\ \mu_B$.

Calculated magnetic moment of MnO were summarized in Table 5.2 in comparison with experiment [12] and previous results by other calculated methods.[13, 14, 15, 16, 17, 18, 19].

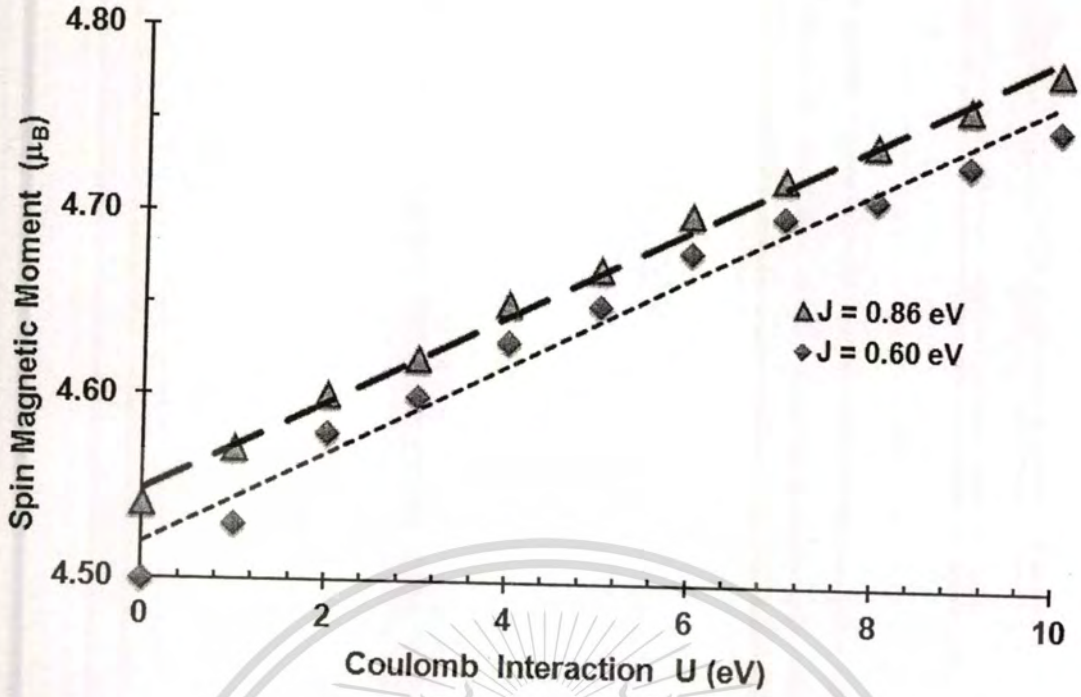

Figure 5.5 The spin magnetic moment of MnO depend on U for J = 0.60 eV and 0.86 eV.

5.5 Effect of the exchange interaction J on magnetic properties of MnO

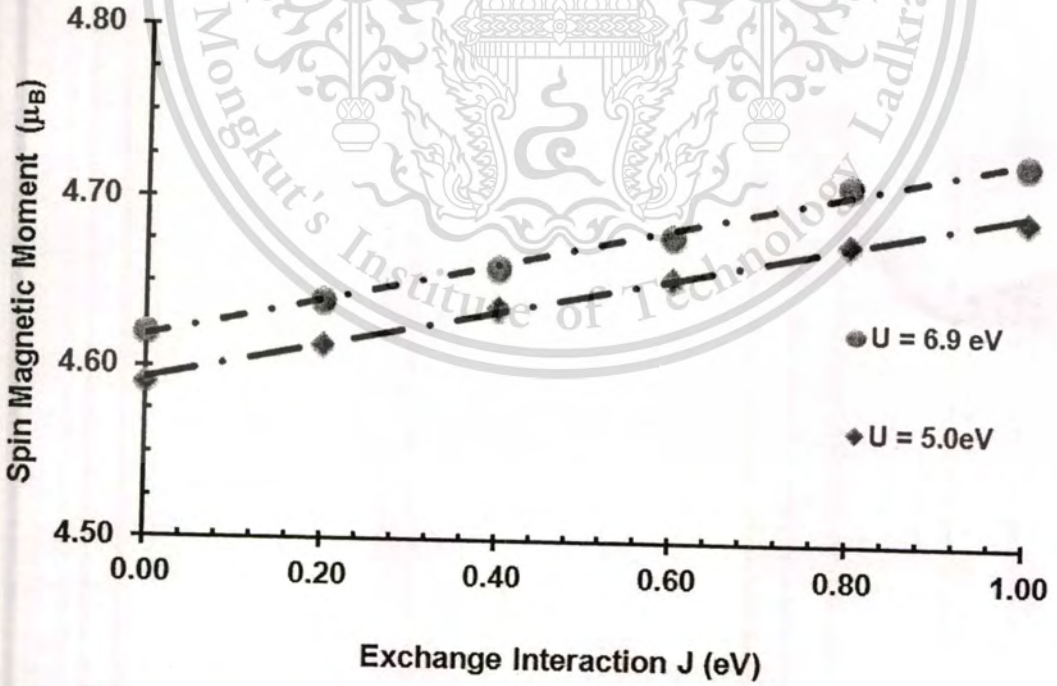

Figure 5.6 The spin magnetic moment of MnO depend on the exchange interaction J for U = 5.0eV and 6.9eV .

Figure 5.6 showed the spin magnetic moments, as a function of J, slightly increased with increasing of J since the exchange interaction J tends to align neighbor spins so the spin magnetic moment increase with increasing of J. The relation of the spin magnetic moment (m_s) and J could be express as $m_s = 0.10J + 4.60\ \mu_B$. In table 5.2 showed our calculated the spin magnetic moment $4.46\,\mu_B$ (U=1.0eV, J =0eV) to $4.78\,\mu_B$ (U =10.0eV, J = 1.0eV). Therefore we can determine that the spin magnetic moment depend on both U and J.

Figure 5.7 showed the relation of U and J where the spin magnetic moment is $4.58\,\mu_B$ [12]. We found that J linearly decreased about 0.25 with increasing of U 1.0eV. Hence, the relation of J and U was obtained : $J = -0.25U + 1.35$ eV. However, the values of spin magnetic moment, were calculated by using LDA+U^{p+d} [20] and Constrained LSDA [21] which both methods used U of 6.9eV and J of 0.86eV were $4.59\,\mu_B$ and $4.61\,\mu_B$, respectively. While our calculation it be equal to $4.58\ \mu_B$, we use J as 0.86eV and 2.0eV of U.

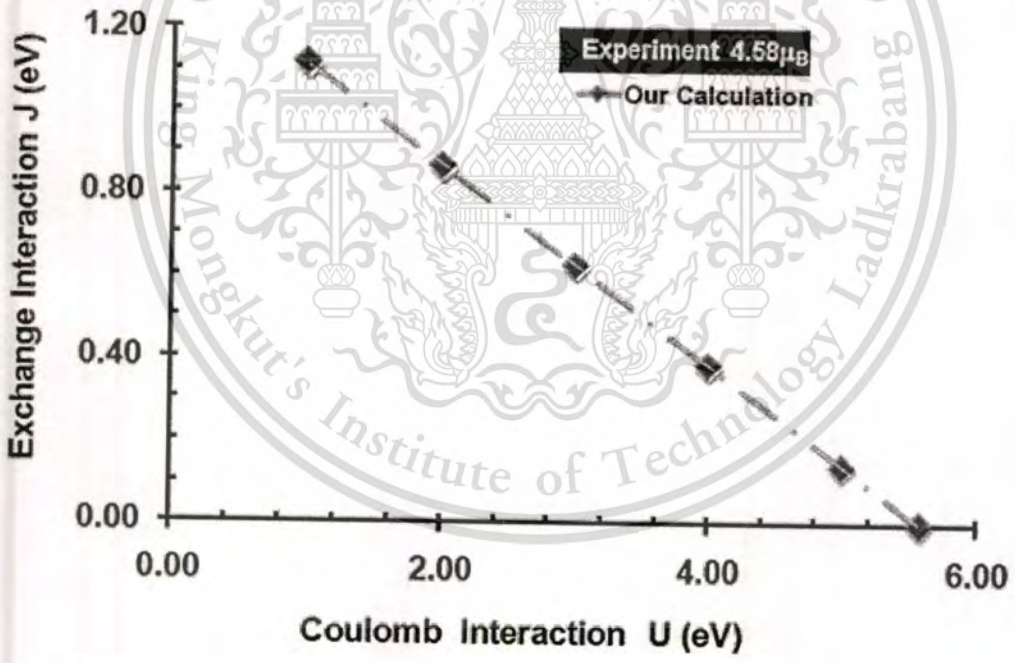

Figure 5.7 The relation of U and J where the spin magnetic moment is $4.58\,\mu_B$.

Table 5.2 Calculated the spin magnetic moment m_s (μ_B), the exchange interaction J (eV) and Coulomb interaction U (eV)

Methods	Coulomb interaction U (eV)	Exchange interaction J (eV)	Spin magnetic moment m_s (μ_B)
Our work : WC	0 – 10	0.86	4.46 - 4.78
	6.9	0-1.0	4.65 – 4.72
Experiment [12]	-	-	4.58
SIC-LSDA-	-	-	4.64
Constrained	6.9	0.86	4.61
LDA+U^{d+p}[15]	6.9	0.86	4.59
Hybrid [16]	-	-	4.46
QP+GW[17]	-	-	4.50
LSIC[18]	-	-	4.63
EXX[19]	-	-	4.81

5.6 Effect of the volume compression *VC* on magnetic properties of MnO

Figure 5.8 shows the variations of the spin (m_s) magnetic moments of MnO as a function of volume compression at U of 6.9.0eV and J of 0.86eV. It is noticed that m_s decrease with increasing *VC*. At the compression range of 0-50%, the m_s decreases from its original value by 1.2% as the *VC* increases by 10%. As the *VC* is larger than 70%, the spin magnetic moment of MnO rapidly decreases to zero. This strange behaviour may be originated from the delocalization of most electrons. This strange phenomena are interesting and still in doubt therefore the further deep researches not only experimental but also theoretical works are required for better clarification.

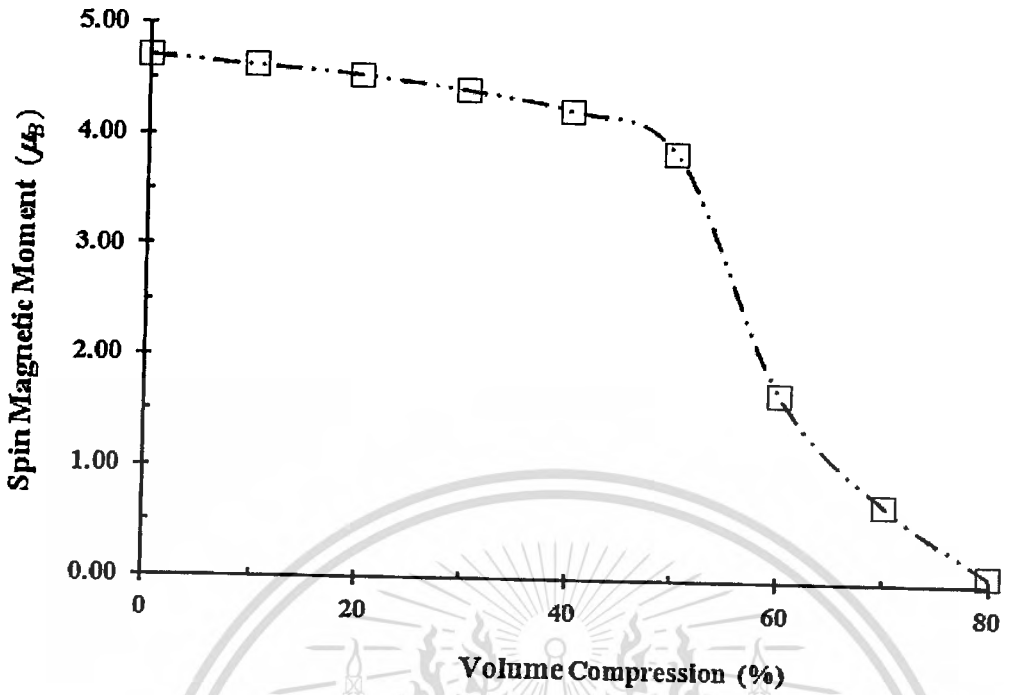

Figure 5.8 The spin magnetic moment of MnO depend on VC at $U = 6.9eV$ and $J = 0.89eV$.

References

[1] S.K. Kwon and B.I. Min, J. Phys. Rev. B 62, 73(2000).

[2]. V. Fernandez, C. Vettier, F. de Bergevin, C. Giles, and W. Neubeck, J. Phys. Rev. B 57, 7870(1998).

[3] J.C. Fuggle, G.A. Sawatzky and J.W. Allen, B. in *Brandow, Narrow Band Phenommena,* Plenum, New York, 1988.

[4] I. Barin, in *Thermochemical Data of Pure Substance*, VCH, Cambrige, (1989).

[5] H. A. Alperin, J. Phys. Soc. Jpn. Suppl. B. 17,12 (1962).

[6] E. Engel and R.N. Schmid, J. Phys. Rev. Lett. 103, 036404(2009).

[7] C. Rodl, F. Fuchs, J. Furthmuller and F. Bechstdedt, J. Phys. Rev B 79,235114(2009).

[8] R.J. Radwanski and Z. Ropka, J. Physica B, 403, 1453(2008).

[9] R.J. Radwanski and Z. Ropka, J. Physica B 345, 107(2004).

[10] B.E.F. Fender, A.J. Jacobson and F.A. Wedgewood, J. Chem. Phys. 48, 990 (1968).

[11] T. Eto, S. Endo, M. Imai, Y. Katayana, and T. Kikegawa, J. Phys. Rev. B. 61, 14984 (2000).

[12]. A.K. Cheetham and D.A. Hope, "Magnetic ordering and exchange effects in the antiferromagnetic solid solutions $Mn_xNi_{1-x}O$", J. Phys. Rev B., 27, pp 6964-6967, 1983.

[13]. Z. Szotek, and .W.M. Temmerman, " Applicaton of the self-interaction correction to transition-metal oxides", J. Phys. Rev. B.47, vol 7, 4029-4032, 1992.

[14]. V.I. Anisimov, J Zaanen and O.K Anderson, " Band Theory and Mott insulators: Hubbard U instead of Stoner I ", J. Phys. Rev. B, 44, vol 3, pp 943-954, 1991.

[15]. I.A. Nekrasov, M.A. Korotin and F. V.I. Anisimov, "cond-mat 0009107v1", 2008.

[16]. F.Tran, P. Blaha, K. Schwarz and P. Novak, "Hybrid exchange-correlation energy functionals for strongly correlated electrons: Applications to transition-metal monoxides", J. Phys. Rev. B. 74, 2006, pp 155108 -155117.

[17]. C. Rodl, F. Fuchs, J. Furthmuller and F. Bechstedt, "Quasiparticle band structures of the antiferromagnetic transition-metal oxides MnO, FeO, CoO, and NiO ", J. Phys. Rev. B.79, pp 235114-235121, 2009.

[18]. G. Fisher, M. Dane, W. Temmerman and W. Hergert, " Exchange coupling in transition metal monoxide : Electronic structure calculations", J. Phys. Rev.B 80, pp 014408-1-014408-11, 2009.

[19]. E. Engel, and R.N. Schmid, " Insulating Ground States of Transition-Metal Monoxides from Exact Exchange " , J. Phys. Rev. Lett 103, pp 036404-1-036404-4,2009.

[20]. I.A. Nekrasov, M.A. Korotin and F. V.I. Anisimov, "cond-mat 0009107v1", 2008.

[21]. V.I. Anisimov, J Zaanen and O.K Anderson, " Band Theory and Mott insulators: Hubbard U instead of Stoner I ", J. Phys. Rev. B, 44, vol 3, pp 943-954, 1991.

CHAPTER 6

CONCLUSIONS AND FURTURE PERSPECTIVES

6.1 Conclusions

This section was explaining the overall results of this dissertation. This work presented a comprehensive study of NiO (nickel oxide) and MnO (manganese oxide). By simplifying of MStudio program within the Coulomb interaction U vary from 0 to 10eV, the exchange interaction J, from 0 to 1.0eV and volume compression VC in range of 0 to 80%. The background of transition metal oxides, the electronic structure and magnetic properties of NiO and MnO were reviewed in chapter 2. Theoretical background of density functional theory (DFT) and the local spin density approximation plus Coulomb interaction (LSDA+U) were briefly described in chapter 3. In chapter 4, we reviewed the structure and details of the LMTART program, which was based on the DFT methods. We discussed the MStudio program and explained the control files that need to be prepared for implementation of the MStudio.

In chapter 5, We assumed NiO as a type II antiferromagnetic with lattice constant a of 0.419 nm. The muffin-tin radii of Ni^{2+} and O^{2-} ions are 2.179 and 1.783 a.u., respectively and self-consistent for minimum energy 30 loop. Effect of the Coulomb interaction U, exchange interaction J and the volume compression on spin and orbital magnetic moment of NiO, that were calculated by using LSDA+U method within FP-LMTO, were obtained. Our results revealed that when the volume compression was increased to 30%, the lattice constant decreased from 0.419 nm to 0.372nm, which affected to the decrease in spin and orbital magnetic moment from $1.78\,\mu_B$ to $1.65\,\mu_B$ and $0.16\,\mu_B$ to $0.10\,\mu_B$, respectively. The relation of magnetic moments and Coulomb interaction could be expressed as $m_s = 0.03U + 1.60\ \mu_B$ and $m_o = 0.003U + 0.14\ \mu_B$. Meanwhile, Both m_s and m_o of NiO also strongly depend on J. So, we can summarize that both spin and orbital magnetic moment increase with increasing Coulomb interaction and exchange interaction, but decrease with increasing volume compression. It is clearly noticed that the values of magnetic moment strongly depend on the U, J and volume compression. Furthermore the evaluated pressure based on LSDA+U method is well agreeable to experimental data. Moreover, at very high pressure (~5 TPa), the volume compression exceeds 80% causing the disappearance of spin and orbital magnetic moments.

The effect of the Coulomb interaction U, the exchange interaction J and volume compression VC on magnetic properties of MnO were studied by using MStudio program with lattice constant a of 0.444 nm, the muffin-tin radii of Mni^{2+} and O^{2-} ions are 2.346 and 1.843 a.u., respectively and self-consistent for minimum energy 10 loop. Our calculated results revealed that the value of the spin magnetic moments depend the J and U. Furthermore we could expressed as $m_s = 0.02U + 4.55\mu_B$ and $m_s = 0.10J + 4.60\mu_B$. The variations of the spin magnetic moments (m_s) of MnO as a function of volume compression, They slightly decreased with increasing VC. At compression range of 0 – 50%, the m_s decreased from its original value by 1.2% as the VC increased by 10%. As the VC was larger than 70%, the spin magnetic moment of NiO and MnO rapidly decreased to zero. This strange behavior maybe originated from the delocalization of most electrons. Moreover, at higher compression, the VC exceed 80% causing the disappearance of magnetic moment.

6.2 Future perspectives

My research interests include computational physics based on first principle, density functional approximation and strongly correlated material.

AUTHOR BIOGRAPHY

Mr. Chewa Thassana was born in Sukhothai Thailand on September 27, 1975. I receive B.Sc. degree in Physics (Computer and electronics) from Naresuan university (NU), Pisaniloke, Thailand in1997 and M.Sc. Degree in Applied Physics from King Mongkut's Institute of Technology Ladkrabang (KMITL), Bangkok, Thailand in 2006. I am now studying toward the Ph.D. degree in Applied Physics at Mongkut's Institute of Technology Ladkrabang (KMITL) Bangkok, Thailand and working with Physics and General Science Program, faculty of science and technology, Nakhon Ratchasima Rajabhat university (NRRU), Nakhonratchasima, Thailand.

My research interests include computational physics based on first principle, density functional theory, strongly correlated material, computational physics and computational science.